RSC Advances

PAPER

View Article Online
View Journal | View Issue

Cite this: RSC Adv., 2016, 6, 31588

VIS and VUV spectroscopy of $^{12}C^{17}O$ and deperturbation analysis of the $A^1\Pi$, $v = 1–5$ levels

R. Hakalla,*[a] M. L. Niu,[b] R. W. Field,[c] E. J. Salumbides,[bd] A. N. Heays,[e] G. Stark,[f] J. R. Lyons,[g] M. Eidelsberg,[h] J. L. Lemaire,†[i] S. R. Federman,[j] M. Zachwieja,[a] W. Szajna,[a] P. Kolek,[a] I. Piotrowska,[a] M. Ostrowska-Kopeć,[a] R. Kępa,[a] N. de Oliveira[k] and W. Ubachs[b]

High-accuracy dispersive optical spectroscopy measurements in the visible (VIS) region have been performed on the less-abundant $^{12}C^{17}O$ isotopologue, observing high-resolution emission bands of the $B^1\Sigma^+$ ($v = 0$) → $A^1\Pi$ ($v = 3$, 4, and 5) Ångström system. These are combined with high-resolution photoabsorption measurements of the $^{12}C^{17}O$ $B^1\Sigma^+$ ($v = 0$) ← $X^1\Sigma^+$ ($v = 0$) and $C^1\Sigma^+$ ($v = 0$) ← $X^1\Sigma^+$ ($v = 0$) Hopfield–Birge bands recorded with the vacuum-ultraviolet (VUV) Fourier transform spectrometer, installed on the DESIRS beamline at the SOLEIL synchrotron. The frequencies of 429 observed transitions have been determined in the 15 100–18 400 cm^{-1} and 86 900–92 100 cm^{-1} regions with an absolute accuracy of up to 0.003 cm^{-1} and 0.005 cm^{-1} for the B–A, and B–X, C–X systems, respectively. These new experimental data were combined with data from the previously analysed C → A and B → A systems. The comprehensive data set, 982 spectral lines belonging to 12 bands, was included in a deperturbation analysis of the $A^1\Pi$, $v = 1–5$ levels of $^{12}C^{17}O$, taking into account interactions with levels in the $d^3\Delta_i$, $e^3\Sigma^-$, $a'^3\Sigma^+$, $I^1\Sigma^-$ and $D^1\Delta$ states. The $A^1\Pi$ and perturber states were described in terms of a set of deperturbed molecular constants, spin–orbit and L-uncoupling interaction parameters, equilibrium constants, 309 term values, as well as isotopologue-independent spin–orbit and rotation-electronic perturbation parameters.

Received 16th January 2016
Accepted 15th March 2016

DOI: 10.1039/c6ra01358a

www.rsc.org/advances

1. Introduction

Carbon monoxide (CO) is one of the most thoroughly studied molecules, bearing significance to astronomy and cosmology. After H_2, it is the second most abundant molecule in the interstellar medium (ISM), where it is investigated as a tracer of gas properties, structure and kinematics.[1,2] In such astrophysical environments CO controls much of the gas-phase chemistry,[3] and is a precursor to complex molecules.[4] The CO spectrum has been observed in comets, cool dwarfs, quasars, supernova remnants, and interstellar molecular clouds as well as in atmospheres of planets and transiting exoplanets.[5,6] Emissions originating from the $B^1\Sigma^+$ ($v = 0$), $B^1\Sigma^+$ ($v = 1$), and $C^1\Sigma^+$ ($v = 0$) vibrational levels were recorded from the Martian and Venusian atmospheres by the Hopkins Ultraviolet Telescope,[7] the *FUSE* satellite,[8,9] and the Cassini UVIS instrument.[10] Large CO abundances produce detectable signals even for the rare isotopologues, including $^{12}C^{17}O$.[11–13] Investigations of minor isotopologues are applied to unravel 'depth effects' in the interstellar absorptions[14] and for precise determination of the $[^{12}C]/[^{13}C]$ and $[^{16}O]/[^{17}O]/[^{18}O]$ ratios in the ISM.[13,15] The CO vacuum ultraviolet absorption spectrum is of astrophysical relevance due to the photodissociation of VUV-excited states, *e.g.* the $C^1\Sigma^+$, $B^1\Sigma^+$ and $E^1\Pi$ states.[16] Isotope-dependent photodissociation effects, due to self-shielding in high-column density environments,[15,17] lead to isotopic fractionation of CO.[13,18]

The less-abundant $^{12}C^{17}O$ isotopologue was detected in the ISM for the first time in 1973 in the Orion Nebula[19] and has been studied in the laboratory in a number of investigations.[20–25]

[a]Materials Spectroscopy Laboratory, Department of Experimental Physics, Faculty of Mathematics and Natural Science, University of Rzeszów, ul. Prof. S. Pigonia 1, 35-959 Rzeszów, Poland. E-mail: hakalla@ur.edu.pl
[b]Department of Physics and Astronomy, and LaserLaB, Vrije Universiteit, De Boelelaan 1081, 1081 HV Amsterdam, Netherlands
[c]Department of Chemistry, Massachusetts Institute of Technology, Cambridge, MA 02139, USA
[d]Department of Physics, University of San Carlos, Cebu City 6000, Philippines
[e]Leiden Observatory, Leiden University, PO Box 9513, 2300 RA Leiden, Netherlands
[f]Department of Physics, Wellesley College, Wellesley, MA 02481, USA
[g]School of Earth and Space Exploration, Arizona State University, PO Box 871404, Tempe, AZ 85287, USA
[h]Observatoire de Paris, LERMA, UMR 8112 du CNRS, 92195 Meudon, France
[i]Institut des Sciences Moléculaires d'Orsay (ISMO), CNRS – Université Paris-Sud, UMR 8214, 1405 Orsay, France
[j]Department of Physics and Astronomy, University of Toledo, Toledo, OH 43606, USA
[k]Synchrotron SOLEIL, Orme de Merisiers, St. Aubin, BP 48, F-91192 Gif sur Yvette Cedex, France
† Previously at Paris Observatory, LERMA.

Table 1 Transition frequencies (in cm^{-1}) of the $^{12}C^{17}O$ $B^1\Sigma^+ \rightarrow A^1\Pi$ emission bands from the high-accuracy dispersive optical spectroscopy measurements[a]

	$B^1\Sigma^+ \rightarrow A^1\Pi$ (0, 3)			$B^1\Sigma^+ \rightarrow A^1\Pi$ (0, 4)			$B^1\Sigma^+ \rightarrow A^1\Pi$ (0, 5)		
J''	$P_{11ee}(J'')$	$Q_{11ef}(J'')$	$R_{11ee}(J'')$	$P_{11ee}(J'')$	$Q_{11ef}(J'')$	$R_{11ee}(J'')$	$P_{11ee}(J'')$	$Q_{11ef}(J'')$	$R_{11ee}(J'')$
1	17873.5415[w]	17877.3487	17884.9340[w]	16511.6992[wb]	16515.4938	16523.0926[wb]	15183.9236[w]	15187.7309[b]	15195.3164[wb]
2	17871.3560[w]	17878.9588	17890.3448[wb]	16509.6030[wb]	16517.1954	16528.5907[w]	15181.9146[wb]	15189.5160	15200.9022[w]
3	17869.9711[b]	17881.3756	17896.5532	16508.3534[b]	16519.7453	16534.9352	15180.8067	15192.1968	15207.3878
4	17869.3988[b]	17884.5914	17903.5738	16507.9558	16523.1441[b]	16542.1318[b]	15180.5825	15195.7723	15214.7562[b]
5	17869.6231[b]	17888.6168	17911.3897	16508.4044[b]	16527.3907	16550.1711	15181.2601	15200.2415	15223.0281[b]
6	17870.6627[b]	17893.4479[b]	17920.0175	16509.7149[b]	16532.4902	16559.0712	15182.8347	15205.6131	[d]
7	17872.5000	17899.0872[b]	17929.4448[b]	16511.8668[b]	16538.4413	16568.8116	15185.3034	15211.8759	15242.2470
8	17875.1495	17905.5280	17939.6817	16514.8754	16545.2370	16579.4055	15188.6753	15219.0329[b]	15253.1997
9	17878.6007	17912.7727	17950.7216	16518.7325	16552.8844	16590.8456	15192.9308	15227.0844	15265.0420
10	17882.8628	17920.8230	17962.5630	16523.4385	16561.3885	16603.1382	[b]	15236.0352	15277.7829
11	17887.9333[b]	17929.6776	17975.2018	16529.0007	16570.7363	16616.2656	15204.1416	15245.8790	15291.4191
12	17893.8041[b]	17939.3388	17988.6474	16535.4121	16580.9368	16630.2435	15211.1034	15256.6216	15305.9482[b]
13	17900.4819	17949.8052	18002.9017	16542.6783	16591.9832[b]	16645.0971	15218.9579[b]	15268.2593	15321.3691
14	17907.9701	17961.0768	18017.9529	16550.7939	16603.8795[b]	16660.7753	15227.7106	15280.7983	15337.6939
15	17916.2705[w]	17973.1496	18033.7998	16559.7665	16616.6342	16677.3045	[c]	15294.2314	15354.9027
16	17925.3745	17986.0335	18050.4689	16569.5907	16630.2435[b]	16694.6922	15247.9101	15308.5584	15373.0036
17	17935.2870[b]	17999.7350[b]	18067.9402	16580.2662	16644.6981	16712.9238	15259.3599	15323.8044	15392.0068
18	17946.0199	18014.2502	18086.2085[b]	16591.8117[b]	16660.0117	16732.0040	15271.7297	15339.9268	15411.9211
19	17957.6189[b]	18029.6005[b]	18105.3502	16604.1975	16676.1770[b]	16751.9305	15284.9971	15356.9602	15432.7399
20	17969.9100	18045.6680	18125.1789	16617.4401	16693.1912	16772.7136	15299.1573	15374.8906	15454.4240
21	17983.0826[b]	18062.6124[b]	18145.8766	16631.5498	16711.0648	16794.3439	15314.2281	15393.7315	15477.0222
22	17997.0654	18080.4029	18167.3898	16646.5087	16729.7939	16816.8168	15330.1972[b]	15413.4733	15500.5139
23	18011.8926	18099.0791	18189.7235	16662.3326	16749.4891	16840.1597[b]	15347.0858	15434.1239	15524.9246[wb]
24	18027.5385	18119.3843	18212.8737	16679.0067	16769.7712	16864.3394[b]	15364.8940	15455.6780	15550.2386[wb]
25	18044.1309	18137.7727[b]	18236.9649	16696.5573	16791.0561	16889.3887[b]	15383.6275	15478.1744[b]	15576.4581[wb]
26	18061.8968	18159.0512[b]	18262.2549	16714.9513[b]	16813.2121	16915.2774[b]	15403.2833[wb]	15501.6332	15603.6053[wb]
27	18076.9080	18180.9483[b]	18284.7404[wb]	16734.2123[b]	16836.2224	16942.0178[b]	15423.9461[w]	[e]	15631.7723[w]
28	18097.1756	18203.6581	18312.4882[wb]	16754.3424[w]	16860.1012	16969.6086	15445.2634[w]	15552.7612[b]	15660.5543[wb]
29	18117.0975[b]	18227.4324	18339.8457[w]	16775.3465[w]	16884.8186	16998.0915[b]		15576.7018[wb]	
30	18137.6823[b]	18250.1705	18367.8876[w]	16797.2108[w]	16910.4095	17027.3687[w]		15604.1346[wb]	
31	18159.0776[wb]	18275.8613[b]	18396.7270[wb]	16819.9516[wb]	16936.8710			15630.5207[w]	
32	18181.1794[wb]	18301.8278[w]		16843.5748[w]	16964.1936			15660.4293[wb]	
33	18204.5622[w]	18328.9618[wb]		16868.2295[w]	16992.3948				
34	18227.8885[w]	18356.0240[wb]		16891.7250[w]	17021.4713[w]				
35	18252.4990[wb]	18384.3289[w]							
36		18413.4754[w]							

	$B^1\Sigma^+ \rightarrow A^1\Pi$ (0, 1)[f]			$B^1\Sigma^+ \rightarrow A^1\Pi$ (1, 5)[f]		
J''	$P_{11ee}(J'')$	$Q_{11ef}(J'')$	$R_{11ee}(J'')$	$P_{11ee}(J'')$	$Q_{11ef}(J'')$	$R_{11ee}(J'')$
1						
…						
21					17438.5662[w]	
22					17457.1157[w]	
23					17476.5644[w]	
…						
35		21150.5933[w]				

[a] The estimated absolute calibration 1σ uncertainty was 0.002 cm^{-1}. Lines marked with 'w' were weak and with 'b' were blended in the spectra. Absolute accuracy of the line frequency measurements varies between 0.003 and 0.07 cm^{-1} for the strongest and weakest lines, respectively. [b] The P(10) line of the B–A(0, 5) band was overlapped by the carbon atomic line at 15197.891 cm^{-1} of significantly higher intensity and half-width. The identification after NIST ASD.[59,60] [c] The P(15) line of the BA(0, 5) band was overlapped by the deuterium atomic line at 15237.272 cm^{-1} of significantly higher intensity and half-width. The identification after NIST ASD.[61,62] [d] The R(6) line of the B–A(0, 5) band was overlapped by the hydrogen atomic line at 15233.157 cm^{-1} (H_α of the Balmer series) of significantly higher intensity and half-width. The identification after NIST ASD.[61,63] [e] The Q(27) line of the B–A(0, 5) band is significantly weakened by multistate, strong perturbations derived from interactions with the $d^3\Delta_i$ ($v = 11$) and $a'^3\Sigma^+$ ($v = 16$) states, by which it was not possible to distinguish this line from the noise. [f] The additionally assigned lines based on better, than in the previous works[26–28] understanding of the spectrum of the $^{12}C^{17}O$. The (1, 5) lines originate from above the first predissociation limit of CO located at 90679.1 cm^{-1}.[64]

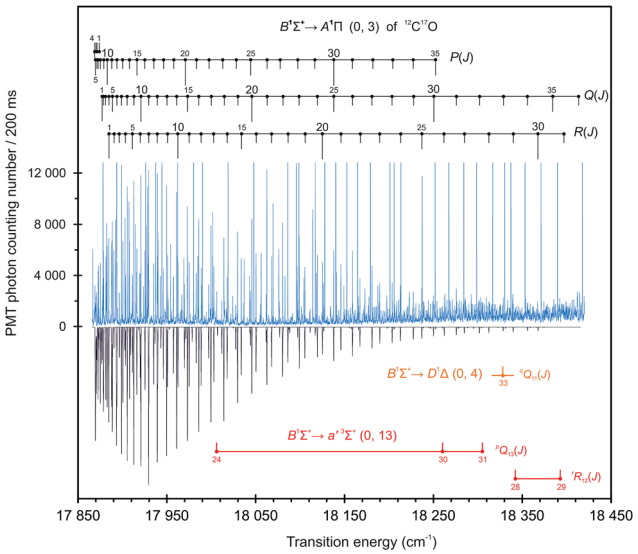

Fig. 1 High resolution emission spectra, recorded with the high-accuracy dispersive optical spectroscopy setup[66] at an instrumental resolution of 0.15 cm^{-1}, of the $^{12}C^{17}O$ $B^1\Sigma^+ \rightarrow A^1\Pi$ (0, 3) band, with the perturber lines associated with the $B^1\Sigma^+ \rightarrow D^1\Delta$ (0, 4), and $B^1\Sigma^+ \rightarrow a'^3\Sigma^+$ (0, 13) transitions (upper trace) together with the final branch assignments, calibrating Th atomic lines (going beyond the scale), as well as simulated spectra[67] (lower trace). The ratio of the gas compositions used to obtain the molecular spectra was $^{12}C^{17}O : {}^{12}C^{16}O = 1 : 0.35$.

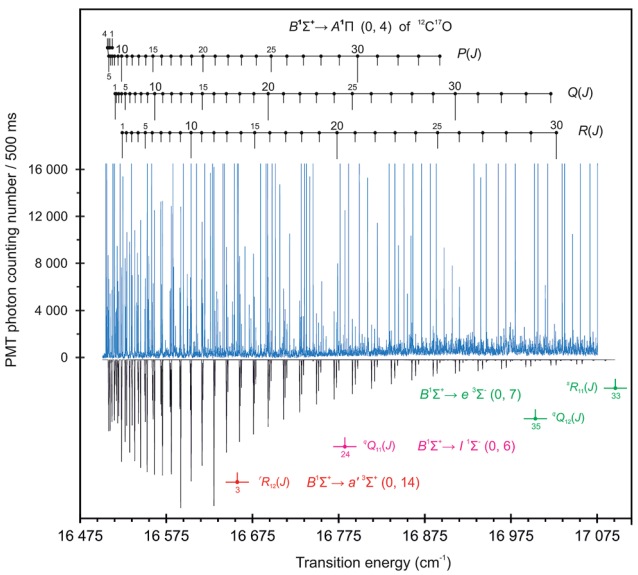

Fig. 2 High resolution emission spectra, recorded with the high-accuracy dispersive optical spectroscopy setup[66] at an instrumental resolution of 0.15 cm^{-1}, of the $^{12}C^{17}O$ $B^1\Sigma^+ \rightarrow A^1\Pi$ (0, 4) band, with the perturber lines associated with the $B^1\Sigma^+ \rightarrow e^3\Sigma^-$ (0, 7), $B^1\Sigma^+ \rightarrow I^1\Sigma^-$ (0, 6), and $B^1\Sigma^+ \rightarrow a'^3\Sigma^+$ (0, 14) transitions (upper trace) together with the final branch assignments, calibrating Th atomic lines (going beyond the scale), as well as simulated spectra[67] (lower trace). The ratio of the gas compositions used to obtain the molecular spectra was $^{12}C^{17}O : {}^{12}C^{16}O = 1 : 0.35$.

Hakalla and co-workers have investigated the visible spectrum of $^{12}C^{17}O$, comprising the $B^1\Sigma^+$–$A^1\Pi$ Ångström system,[26,27] as well as the $C^1\Sigma^+$–$A^1\Pi$ Herzberg system.[28] The VUV spectrum of the $C^1\Sigma^+$–$X^1\Sigma^+$ system was investigated by laser excitation[22,29] and the $B^1\Sigma^+$–$X^1\Sigma^+$ system by absorption of synchrotron radiation.[25]

The $A^1\Pi$ state is subject to some of the most extensive and complex perturbations among all the states that are known in the carbon monoxide molecule.[30–38] The $d^3\Delta_i$, $e^3\Sigma^-$, $a'^3\Sigma^+$, $I^1\Sigma^-$, and $D^1\Delta$ electronic states are responsible for all of the existing irregularities. A systematic classification of the perturbations of

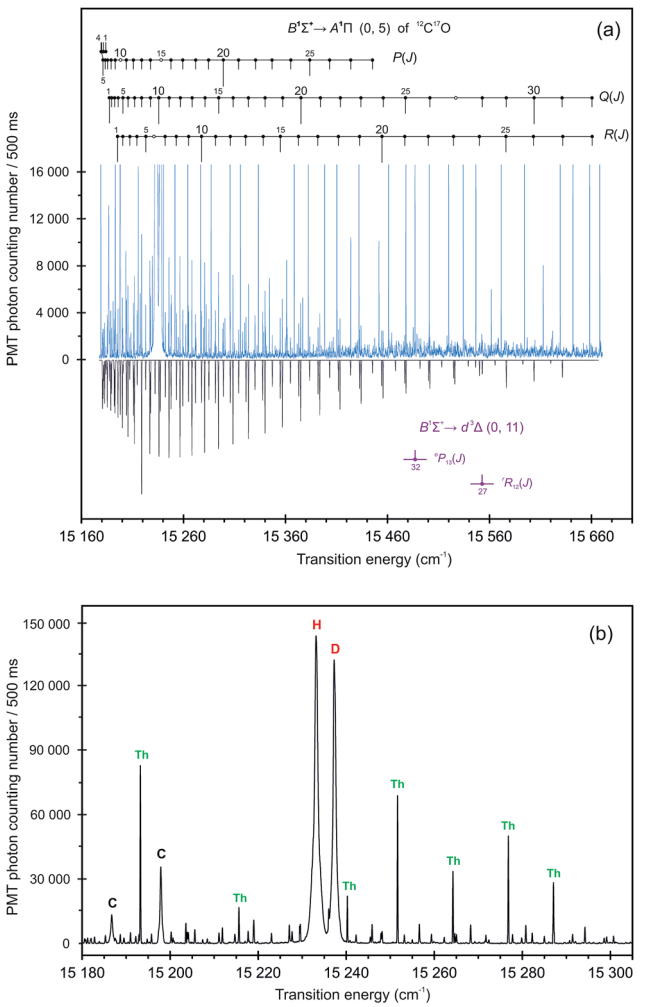

Fig. 3 High resolution emission spectra, recorded with the high-accuracy dispersive optical spectroscopy setup[66] at an instrumental resolution of 0.15 cm^{-1}, of the $^{12}C^{17}O$ $B^1\Sigma^+ \rightarrow A^1\Pi$ (0, 5) band with the perturber lines associated with the $B^1\Sigma^+ \rightarrow d^3\Delta$ (0, 11) transition. The ratio of the gas compositions used to obtain the molecular spectra was $^{12}C^{17}O : {}^{12}C^{16}O = 1 : 0.35$. (Panel (a)) An overview of the observed $B^1\Sigma^+ \rightarrow A^1\Pi$ (0, 5) and $B^1\Sigma^+ \rightarrow d^3\Delta$ (0, 11) spectra (upper trace) together with the final branch assignments, calibrating Th atomic lines (going beyond the scale), as well as simulated spectra[67] (lower trace). The empty circles indicate spectral lines of undetermined location due to overlap with much more intense atomic lines of carbon, hydrogen, and deuterium. (Panel (b)) Expanded view of the B → A (0, 5) band head region in $^{12}C^{17}O$ at an enlarged scale.

the $A^1\Pi$ state in the main $^{12}C^{16}O$ molecule was carried out by Krupenie.[39] Simmons *et al.*[40] made a critical analysis of this study as well as completed it. A conclusive analysis and deperturbation calculations were carried out by Field *et al.*[30,32,41] Next, Le Floch *et al.*[31] conducted a comprehensive study of perturbations in the lowest $A^1\Pi$, $v = 0$ vibrational level. In his next works[42,43] he analysed perturbations occurring in the $A^1\Pi$, $v =$ 0–4 levels, and calculated very precise term values for the $A^1\Pi$, $v = 0$–8 states, respectively. Recently, the $A^1\Pi$ state of the main $^{12}C^{16}O$ isotopologue has been studied in the A–X transition[44–46] by the Amsterdam group by means of highly accurate two-photon Doppler-free excitation using narrow band lasers[47] with relative accuracy up to $\Delta\lambda/\lambda = 2 \times 10^{-8}$, as well as by vacuum ultraviolet Fourier-transform spectroscopy (VUV-FTS) at the SOLEIL synchrotron.[48–50] An improved deperturbation analysis of $A^1\Pi$ in ordinary CO has recently been performed by Niu *et al.*[44,51] Far fewer deperturbation analyses of the $A^1\Pi$ state have been performed in other isotopologues of CO ($^{12}C^{18}O$ and $^{13}C^{18}O$).[33,52,53] A considerable contribution to the identification and classification of the $A^1\Pi$ state perturbations has been made by Kępa and Rytel in a number of investigations over the years.[54–58]

Here, the focus is on a deperturbation analysis of the $A^1\Pi$ ($v = 1$, 2, 3, 4, and 5) levels in the $^{12}C^{17}O$ isotopologue. The deperturbation is based on new observations of the $^{12}C^{17}O$ B → A (0, 3), (0, 4), (0, 5) bands recorded in visible emission at high resolution and previously published studies of the Ångström[26,27] and Herzberg bands.[28] The deperturbation analysis prompted some reassignment of lines in the B–A and C–A systems. New, highly accurate measurements of the $^{12}C^{17}O$ B ← X (0, 0) and C ← X (0, 0) transitions with VUV-FTS were performed and included in the study in order to (i) establish and verify that B ($v = 0$) and C ($v = 0$) levels are unperturbed, and that our perturbation analysis of A-state is not affected by shifts in the upper states, (ii) include an independent set of improved constants, therewith level energies, of B ($v = 0$) and C ($v = 0$), as well as (iii) determine level energies of A-state with respect to ground state of CO. The comprehensive fit on B–A, C–A, B–X, and C–X systems allowed us to perform the most accurate deperturbed rotational constants of the states under consideration.

2. Experimental details

2.1. Emission spectra of the $B^1\Sigma^+ \rightarrow A^1\Pi$ system

In this study, a water-cooled, hollow-cathode lamp with two anodes[65] and a high-accuracy dispersive optical spectroscopy method were used for a high-resolution spectroscopic investigation of the $^{12}C^{17}O$ $B^1\Sigma^+$ ($v = 0$) → $A^1\Pi$ ($v = 3$, 4, and 5) bands in the visible region. The lamp was initially filled with a mixture of helium and acetylene $^{12}C_2D_2$ (Cambridge Isotopes, ^{12}C 99.99%) under the pressure of approximately 6 Torr. An electric current was passed through the mixture for about 200 h, after which a small quantity of ^{12}C carbon became deposited on the electrodes. Subsequently, the lamp was evacuated and

Table 2 Transition frequencies of the ($B^1\Sigma^+$, $C^1\Sigma^+$) → ($d^3\Delta_i$, $e^3\Sigma^-$, $a'^3\Sigma^+$, $I^1\Sigma^-$, and $D^1\Delta$) extra-line bands in $^{12}C^{17}O$[a,b]

System	Band	Branch	J''	Frequency (cm^{-1})	B–A or C–A band of occurrence
$B^1\Sigma^+ \rightarrow d^3\Delta_i$	(0, 7)	$^qP_{13ee}$	35	19632.935	$B^1\Sigma^+$–$A^1\Pi$ (0, 2)
	(0, 11)	$^oP_{11ee}$	32	15487.171^w	$B^1\Sigma^+$–$A^1\Pi$ (0, 5)
		$^rR_{12ee}$	27	15552.369	
$B^1\Sigma^+ \rightarrow e^3\Sigma^-$	(0, 4)	$^qQ_{12ef}$	25	19460.541^w	$B^1\Sigma^+$–$A^1\Pi$ (0, 2)
		$^qP_{11ee}$	26	19463.325^w	
	(0, 7)	$^qQ_{12ef}$	35	17002.628^w	$B^1\Sigma^+$–$A^1\Pi$ (0, 4)
		$^sR_{11ee}$	33	17098.203^{wb}	
$B^1\Sigma^+ \rightarrow a'^3\Sigma^+$	(0, 10)	$^pP_{12ee}$	20	20761.828^w	$B^1\Sigma^+$–$A^1\Pi$ (0, 1)
		$^pP_{12ee}$	22	20820.661	
	(0, 13)	$^pQ_{13ef}$	24	18005.897^w	$B^1\Sigma^+$–$A^1\Pi$ (0, 3)
		$^pQ_{13ef}$	30	18260.250^w	
		$^pQ_{13ef}$	31	18307.498^w	
		$^rR_{12ee}$	28	18342.563	
		$^rR_{12ee}$	29	18392.832	
	(0, 14)	$^rR_{12ee}$	3	16658.293^w	$B^1\Sigma^+$–$A^1\Pi$ (0, 4)
$B^1\Sigma^+ \rightarrow I^1\Sigma^-$	(0, 3)	$^qQ_{11ef}$	7	19291.955	$B^1\Sigma^+$–$A^1\Pi$ (0, 2)
	(0, 6)	$^qQ_{11ef}$	24	16783.703^w	$B^1\Sigma^+$–$A^1\Pi$ (0, 4)
$B^1\Sigma^+ \rightarrow D^1\Delta$	(0, 1)	$^qQ_{11ef}$	27	20986.818^w	$B^1\Sigma^+$–$A^1\Pi$ (0, 1)
	(0, 4)	$^qQ_{11ef}$	33	18327.789^{wb}	$B^1\Sigma^+$–$A^1\Pi$ (0, 3)
$C^1\Sigma^+ \rightarrow e^3\Sigma^-$	(0, 4)	$^qP_{11ee}$	25	24430.966^w	$C^1\Sigma^+$–$A^1\Pi$ (0, 2)
		$^qP_{11ee}$	29	24578.958^w	
$C^1\Sigma^+ \rightarrow a'^3\Sigma^+$	(0, 10)	$^rQ_{11ef}$	22	25952.917^{wb}	$C^1\Sigma^+$–$A^1\Pi$ (0, 1)
	(0, 13)	$^rQ_{11ef}$	24	23111.431	$C^1\Sigma^+$–$A^1\Pi$ (0, 3)
$C^1\Sigma^+ \rightarrow D^1\Delta$	(0, 1)	$^pP_{11ee}$	26	25849.807^w	$C^1\Sigma^+$–$A^1\Pi$ (0, 1)

[a] The estimated calibration 1σ uncertainty was 0.002 cm^{-1}. The absolute accuracy of the significant majority of extra-lines should be assumed as not better than approximately 0.01 cm^{-1} due to their weakness. [b] Lines marked with 'w' were weak and with 'b' were blended in the spectra. The superscript o, p, r, s, or q preceding the main notation P, Q, R of the branch indicates the change in total angular momentum excluding spin for transition to the perturber state.[68]

Table 3 Extended and corrected assignment[a] of some of heavily perturbed or extremely weak lines located mostly in the region of strong and multistate interactions[b,c]

System	J''	Branch	Frequency (cm^{-1})
$B^1\Sigma^+$–$A^1\Pi$ (0, 1)	1	Q_{11ef}	20701.471[wb]
	2	Q_{11ef}	20702.936[w]
	5	Q_{11ef}	20711.661[b]
	26	P_{11ee}	20855.286[b]
	26	R_{11ee}	21055.609[b]
	34	Q_{11ef}	21128.729[b]
$B^1\Sigma^+$–$A^1\Pi$ (0, 2)	26	R_{11ee}	19640.375
	28	Q_{11ef}	19587.541
	29	Q_{11ef}	19600.539
	30	Q_{11ef}	19624.714
	31	Q_{11ef}	19648.885[w]
	31	P_{11ee}	19534.375[wb]
	32	Q_{11ef}	19673.557[w]
	32	P_{11ee}	19550.099[wb]
	33	Q_{11ef}	19698.930[w]
	33	P_{11ee}	19573.885[w]
$B^1\Sigma^+$–$A^1\Pi$ (1, 1)	1	P_{11ee}	22754.143[wb]
	1	R_{11ee}	22765.387[wb]
$B^1\Sigma^+$–$A^1\Pi$ (1, 5)	2	R_{11ee}	17257.095[b]
	21	P_{11ee}	17360.067[wb]
$C^1\Sigma^+$–$A^1\Pi$ (0, 1)	26	P_{11ee}	25855.228[wb]
	26	Q_{11ef}	25953.327
	26	R_{11ee}	26055.176[w]
$C^1\Sigma^+$–$A^1\Pi$ (0, 2)	27	Q_{11ef}	24561.747[b]
	28	Q_{11ef}	24586.932[wb]
	29	Q_{11ef}	24599.645[w]
	30	Q_{11ef}	24623.687[w]
$C^1\Sigma^+$–$A^1\Pi$ (0, 3)	11	P_{11ee}	22889.944[b]
	15	R_{11ee}	23035.165
	16	P_{11ee}	22926.873[b]
	20	P_{11ee}	22970.859
	25	R_{11ee}	23236.712[w]

[a] Extended and corrected assignment of the lines already published in previous publication (ref. 26–28). [b] The estimated calibration 1σ uncertainty was 0.002 cm^{-1}. The absolute accuracy of the significant majority of the lines should be assumed as not better than approximately 0.01 cm^{-1}. [c] Lines marked with 'w' were weak and with 'b' were blended in the spectra.

oxygen containing the $^{17}O_2$ isotope (Sigma-Aldrich, $^{17}O_2$ 60%) was admitted at a static gas pressure of 2 Torr. The anodes were operated at 2 × 650 V and 2 × 50 mA dc. During the discharge process the $^{17}O_2$ molecules decay into atomic oxygen, which then combine with ^{12}C-carbon atoms, ejected from the outer layer of the cathode, thus forming the $^{12}C^{17}O$ molecules in the gas phase. The temperature of the plasma formed at the centre of the cathode was about 600–700 K. These conditions were found to be optimal for the production of CO molecular spectra under control of isotopic composition. The experimental equipment of the Rzeszów laboratory, where these measurements were conducted, has been described in detail by Hakalla *et al.*[66]

Spectroscopic measurements were made by means of a 2 m Ebert plane-grating spectrograph equipped with a 651.5 grooves per mm grating with a total of 45 600 grooves, blazed at 1.0 μm in 3rd and 4th order, giving reciprocal dispersion and resolving power in the ranges 0.11–0.19 nm mm^{-1} and 182 400–136 800, respectively. Discharge emission signals were recorded by means of a photomultiplier tube (HAMAMATSU R943-02) mounted on a linear stage (HIWIN KK5002) along the focal curve of the spectrograph. The input and exit slits were 35 μm in width. The intensities of the lines were measured by means of photon counting (HAMAMATSU C3866 photon counting unit and M8784 photon counting board) with a counter gate time of 200–500 ms (no dead time between the gates). The position of the exit slit was measured by means of a He–Ne laser interferometer (LASERTEX) synchronized with the photon counting board. During one exposure of the counter gate, the position was measured 64 times. Simultaneously recorded thorium atomic lines,[69] obtained from an auxiliary water-cooled, hollow-cathode tube filled with Th foil were used for absolute CO wavenumber calibration.

The peak positions of spectral lines were derived by means of a least-squares procedure assuming a Gaussian line-shape for each spectral contour (30 points per line), with a fitting

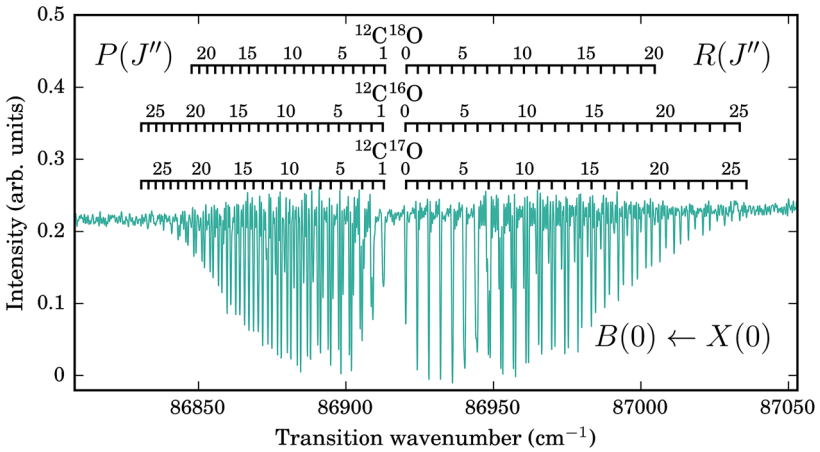

Fig. 4 High resolution absorption spectrum of the $B^1\Sigma^+ \rightarrow X^1\Sigma^+$ (0, 0) Hopfield–Birge band system in the less-abundant $^{12}C^{17}O$ isotopologue recorded with the VUV-FTS setup at the SOLEIL synchrotron at an instrumental resolution of 0.20 cm^{-1}. The estimated absolute calibration 1σ uncertainty was 0.005 cm^{-1}. The 1σ uncertainty due to fitting errors of measured wavenumbers (exclusive of calibration uncertainty) was estimated from the least-squares optimisation algorithm and varies between 0.002 and 0.1 cm^{-1} for the strongest and weakest lines, respectively. The ratio of the gases used in the experiment was $^{12}C^{17}O : {}^{12}C^{16}O : {}^{12}C^{18}O = 1 : 0.85 : 0.20$.

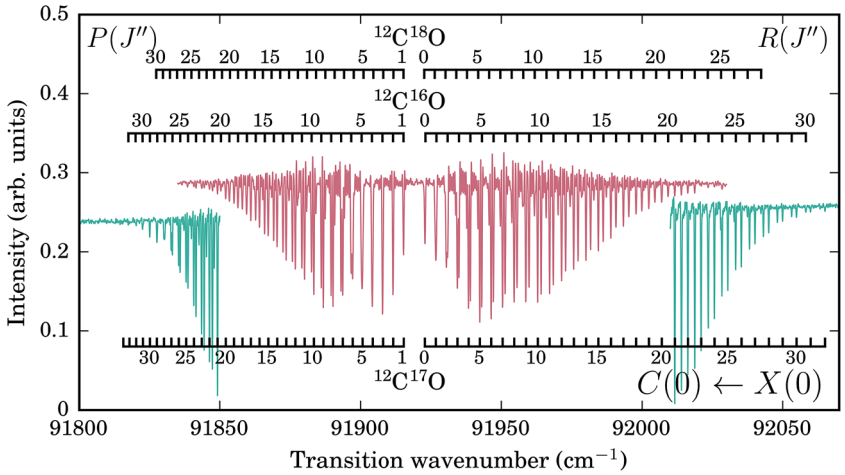

Fig. 5 High resolution absorption spectra of the $C^1\Sigma^+ \rightarrow X^1\Sigma^+$ (0, 0) Hopfield–Birge band system in the less-abundant $^{12}C^{17}O$ isotopologue recorded with the VUV-FTS setup at the SOLEIL synchrotron at an instrumental resolution of 0.20 cm^{-1}. We used two scans at different column density for the lower (red spectrum) and higher (green spectrum) J to get the final list of transition wavenumbers. The estimated absolute calibration 1σ uncertainty was 0.005 cm^{-1}. The 1σ uncertainty due to fitting errors of measured wavenumbers (exclusive of calibration uncertainty) was estimated from the least-squares optimisation algorithm and varies between 0.002 and 0.1 cm^{-1} for the strongest and weakest lines, respectively. The ratio of the gases used in the experiment was $^{12}C^{17}O : {}^{12}C^{16}O : {}^{12}C^{18}O = 1 : 0.85 : 0.20$.

uncertainty of the peak position for a single unblended line in the range 0.1–0.2 μm, that is 2.5–8 × 10^{-4} cm^{-1} in the observed region. To determine the $^{12}C^{17}O$ $B^1\Sigma^+ \rightarrow A^1\Pi$ wavenumbers, 5th- and 6th-order interpolation polynomials were used for the (0, 3), (0, 4), and (0, 5) bands. The absolute wavenumber calibration at 1σ uncertainty is 0.002 cm^{-1}. The strong and unblended lines exhibit a full-width half-maximum (FWHM) of 0.15 cm^{-1}, maximum signal-to-noise ratio of about 100 : 1 as well as count rates of up to about 16 000–60 000 photons per s for the $^{12}C^{17}O$ $B^1\Sigma^+$ ($v = 0$) → $A^1\Pi$ ($v = 3$, 4, and 5) bands. The absolute accuracy of the frequency measurements was 0.003 cm^{-1}, corresponding to a relative accuracy of $\Delta\lambda/\lambda = 2 \times 10^{-7}$, for the 15 180–18 400 cm^{-1} spectral region. However, weaker or blended lines have lower accuracy, at worst 0.07 cm^{-1} or $\Delta\lambda/\lambda = 4 \times 10^{-6}$.

Preliminary identification of the $B^1\Sigma^+$ ($v = 0$) → $A^1\Pi$ ($v = 3$, 4, and 5) bands was carried out by means of the information provided in our recent works on the $^{12}C^{17}O$ molecule.[26,27] For the frequency measurements of the lines investigated, blending effects of the $^{12}C^{16}O$ Ångström system were taken into account. They occur as a result of using oxygen $^{17}O_2$ with spectral purity of only 60%. In total, 283 emission lines belonging to the $B^1\Sigma^+ \rightarrow A^1\Pi$ band system in $^{12}C^{17}O$ were identified and rotationally assigned. The transition frequencies are provided in Table 1. The observed $^{12}C^{17}O$ $B^1\Sigma^+$ ($v = 0$) → $A^1\Pi$ ($v = 3$, 4, and 5) spectra, together with extra-lines, assignments, calibrating Th atomic lines, and final simulated spectra are shown in Fig. 1–3. By "extra-lines", we refer to the spectral emission lines terminating on perturber states and gaining intensity from mixing with the $A^1\Pi$ state. An additional impediment was the appearance of four atomic lines overlapping the region of the $^{12}C^{17}O$ B → A (0, 5) band with significantly higher intensities and broader FWHMs. They were identified by means of the Atomic Spectra Database (ASD) of NIST[59–63] as the C lines at 15186.739 cm^{-1} and 15197.891 cm^{-1}, as well as the H Balmer-alpha line at 15233.157 cm^{-1} and deuterium D line at 15237.272 cm^{-1}. As a result, it was not possible to measure the positions of the P(11), P(15), and R(6) B → A (0, 5) lines (marked with empty circles in Fig. 3a).

Our deperturbation analysis allowed us to assign 24 rotational lines from 14 bands of the $B^1\Sigma^+ \rightarrow d^3\Delta_i$, $B^1\Sigma^+ \rightarrow e^3\Sigma^-$, $B^1\Sigma^+ \rightarrow a'^3\Sigma^+$, $B^1\Sigma^+ \rightarrow I^1\Sigma^-$, $B^1\Sigma^+ \rightarrow D^1\Delta$, $C^1\Sigma^+ \rightarrow e^3\Sigma^-$, $C^1\Sigma^+ \rightarrow a'^3\Sigma^+$, and $C^1\Sigma^+ \rightarrow D^1\Delta$ systems in $^{12}C^{17}O$. The transition frequencies and assignments are presented in Table 2. Since most of them are weak their accuracy is not better than 0.01 cm^{-1}. The deperturbation included some lines from the $^{12}C^{17}O$ $B^1\Sigma^+ \rightarrow A^1\Pi$ (0, 1) and (1, 5) bands which we have measured with an improved accuracy[26–28] and reassigned. Lines in the B → A (1, 5) band originate from above the first dissociation limit of CO located at 90679.1 cm^{-1},[64] and have low intensities due to the competition of emission with predissociation.[70] The wavelengths for these lines are collected in Table 1. All high-J lines located in the perturbation regions, previously analysed[26–28] in $^{12}C^{17}O$, were checked carefully with regard to their quality, because these lines are usually weak. Those lines that were too weak and/or blended were removed from the deperturbation analysis. Also, we extended and corrected the assignment of some heavily perturbed or extremely weak lines located in the region of strong and multistate interactions. They are collected in Table 3.

2.2. VUV-FTS of the $B^1\Sigma^+ \leftarrow X^1\Sigma^+$ and $C^1\Sigma^+ \leftarrow X^1\Sigma^+$ systems

We have measured photoabsorption spectra for two bands of $^{12}C^{17}O$: $B^1\Sigma^+ \leftarrow X^1\Sigma^+$ (0, 0) and $C^1\Sigma^+ \leftarrow X^1\Sigma^+$ (0, 0). Their spectra, shown in Fig. 4 and 5, respectively, were recorded at the SOLEIL synchrotron utilising the tunable-undulator radiation source of the DESIRS beamline and its permanently-installed vacuum-ultraviolet Fourier-transform spectrometer. The

Table 4 Transition frequencies (in cm^{-1}) of the $^{12}C^{17}O$ $B^1\Sigma^+ \leftarrow X^1\Sigma^+$, and $C^1\Sigma^+ \leftarrow X^1\Sigma^+$ absorption bands from the VUV-FTS measurements[a]

	$B^1\Sigma^+ \leftarrow X^1\Sigma^+$ (0, 0)		$C^1\Sigma^+ \leftarrow X^1\Sigma^+$ (0, 0)	
J''	P(J'')	R(J'')	P(J'')	R(J'')
0		86920.218[bw]		91922.750[bw]
1	86912.686[bw]	86924.067[bw]	91915.194[bw]	91926.567[bw]
2	86908.974[b]	86927.963[b]	91911.507[b]	91930.435[b]
3	86905.328[b]	86931.904[b]	91907.829	91934.341[b]
4	86901.729[b]	86935.904	91904.201	91938.297[b]
5	86898.177[b]	86939.949	91900.614	91942.290[b]
6	86894.685	86944.041	91897.078	91946.322[b]
7	86891.238	86948.186	91893.580	91950.395
8	86887.842	86952.377	91890.124	91954.508
9	86884.500	86956.615	91886.709	91958.664
10	86881.206	86960.907	91883.337	91962.856
11	86877.962	86965.233	91880.012	91967.087
12	86874.775	86969.616	91876.725	91971.365
13	86871.626	86974.045	91873.481	91975.675
14	86868.537	86978.519	91870.286	91980.024
15	86865.497	86983.035	91867.128	91984.412
16	86862.507	86987.601	91864.012	91988.841
17	86859.563	86992.220	91860.940	91993.310
18	86856.674	86996.888	91857.913	91997.811
19	86853.842	87001.572	91854.931	92002.351
20	86851.065	87006.309	91851.987	92006.928
21	86848.308	87011.127	91849.087	92011.547
22	86845.611	87015.940	91846.230	92016.204
23	86843.001	87020.864[w]	91843.421	92020.903
24	86840.392[w]	87025.729[w]	91840.656	92025.634
25	86837.900[w]	87030.662[w]	91837.939	92030.404
26	86835.356[w]	87035.627[w]	91835.262	92035.207
27	86832.887[w]		91832.630	92040.062
28	86830.458[w]		91830.039[w]	92044.939[bw]
29			91827.507[w]	92049.860[bw]
30			91825.005[w]	92054.804[bw]
31			91822.556[w]	92059.793[bw]
32			91820.138[w]	92064.829[bw]
33			91817.774[w]	
34			91815.466[w]	

[a] The estimated absolute calibration 1σ uncertainty was 0.005 cm^{-1}. Lines marked with 'w' were weak, and with 'b' were blended in the spectra. Absolute accuracy of the line frequency measurements varies between 0.002 and 0.1 cm^{-1} for the strongest and weakest lines, respectively.

characteristics of the beamline and spectrometer are described by Nahon *et al.*[50] and de Oliveira *et al.*[48,49] Two room-temperature spectra were recorded with approximate column densities of 2×10^{15} and 6×10^{13} cm^{-2}, and have spectral resolutions of 0.32 and 0.21 cm^{-1} FWHM, respectively. The lower column density measurement was necessary to avoid saturation of the strongest rotational transitions of $C^1\Sigma^+ \leftarrow X^1\Sigma^+$ (0, 0) (as indicated in Fig. 5), and was also used by Stark *et al.*[25] to determine the oscillator strength of this band.

There is significant admixture of the $^{12}C^{16}O$ and $^{12}C^{18}O$ isotopologues in our gas sample[25] and lines from these isotopologues frequently overlap the transitions of $^{12}C^{17}O$. Despite this, we were able to fit wavenumbers with an accuracy better than 0.01 cm^{-1} for many $^{12}C^{17}O$ transitions by modelling the sinc-function line broadening inherent to Fourier-transform spectrometry, as previously implemented and shown with multiple independent codes.[25,71–73] A brief summary of the steps involved in our spectral modelling is as follows:

- An initial wavenumber and integrated cross section was assigned to every observed rotational transition in a recorded B $\leftarrow$ X or C $\leftarrow$ X band, and assuming a column density for each isotopologue component of our spectrum.
- A Gaussian wavelength-dependent cross section for each simulated line was calculated from these values, assuming a Doppler width characteristic of the known experimental temperature (FWHM of 0.20 cm^{-1} for the case of $^{12}C^{17}O$ and 295 K). The summation of all lines provided a total cross section.
- The total cross section was converted into a transmission spectrum by the Beer–Lambert law, then convolved with a sinc function to represent the known instrumental broadening of the FTS, and multiplied by the slightly wavelength dependent synchrotron beam intensity, giving a completely simulated absorption spectrum.
- The simulated spectrum was compared with the raw experimental data and model line wavenumbers and cross sections, and isotopologue column densities, were adjusted to minimise the model-to-experiment difference in a pointwise least-squares sense.

The wavenumbers of $^{12}C^{16}O$ and $^{12}C^{18}O$ B $\leftarrow$ X (0, 0) and C $\leftarrow$ X (0, 0) transitions were determined by the analysis of separate spectra recorded with pure samples of those gases. Additionally, the oscillator strengths of the two bands were shown to be independent of isotopic composition and have the rotational dependence of unperturbed $^1\Sigma^+ \leftarrow {}^1\Sigma^+$ transitions.[25] Thus, we could fix all details of the individual $^{12}C^{16}O$ and $^{12}C^{18}O$ lines in our mixed-gas spectrum while fitting the $^{12}C^{17}O$ lines. The final assessment of column densities allowed us to estimate the admixture of isotopologues in our mixed sample to be $^{12}C^{17}O : {}^{12}C^{16}O : {}^{12}C^{18}O = 1 : 0.85 : 0.20$. The residual error, after optimally fitting B $\leftarrow$ X (0, 0), is nearly consistent with the statistical noise.

Absolute wavenumber calibrations of our spectra were made by comparing lines appearing from contaminant species with their literature wavenumbers: H_2 (ref. 74), Xe (ref. 75 and 76), H (ref. 77), and O (ref. 77). The estimated absolute calibration 1σ uncertainty was 0.005 cm^{-1}. The 1σ uncertainty due to fitting errors of measured wavenumbers (exclusive of calibration uncertainty) was estimated from the least-squares optimisation algorithm and varies between 0.002 and 0.1 cm^{-1} for the strongest and weakest lines, respectively. A listing of 122 measured transition wavenumbers is given in Table 4.

3. Results

3.1. Level energies

Rovibronic term values of the $B^1\Sigma^+$ ($v = 0$) and $C^1\Sigma^+$ ($v = 0$) Rydberg states, with regard to the lowest $X^1\Sigma^+$ ($v = 0$) rovibrational level of the $^{12}C^{17}O$ ground state, were calculated by using the B $\leftarrow$ X (0, 0) and C $\leftarrow$ X (0, 0) transition frequencies obtained from a VUV-FTS experiment and using the ground state molecular parameters by Coxon *et al.*,[80] given for the $^{12}C^{17}O$

Table 5 Rovibronic term values of the $A^1\Pi$ ($v = 1$, 2, 3, 4, and 5), $C^1\Sigma^+$ ($v = 0$), and $B^1\Sigma^+$ ($v = 0$) levels in $^{12}C^{17}O$[a,b]

	$C^1\Sigma^+$ ($v = 0$)	$B^1\Sigma^+$ ($v = 0$)	$A^1\Pi$ ($v = 1$)		$A^1\Pi$ ($v = 2$)		$A^1\Pi$ ($v = 3$)		$A^1\Pi$ ($v = 4$)		$A^1\Pi$ ($v = 5$)	
J	e	e	e	f	e	f	e	f	e	f	e	f
0	91918.942	86916.434										
1	91922.750	86920.218	66218.823	66218.768	67646.816	67646.811	69042.885	69042.875	70404.726	70404.724	71732.502	71732.487
2	91930.315	86927.815	66224.934	66224.893	67652.915	67652.884	69048.887	69048.872	70410.616	70410.619	71738.304	71738.299
3	91941.679	86939.206	66234.132	66234.094	67662.016	67662.007	69057.847	69057.840	70419.456	70419.461	71747.005	71747.010
4	91956.828	86954.390	66246.395	66246.371	67674.177	67674.143	69069.812	69069.808	70431.250	70431.246	71758.624	71758.618
5	91975.774	86973.381	66261.742	66261.739	67689.355	67689.329	69084.774	69084.776	70445.991	70445.990	71773.132	71773.140
6	91998.503	86996.162	66280.161	66280.154	67707.592	67707.529	69102.724	69102.720	70463.666	70463.672	71790.546	71790.549
7	92025.018	87022.737	66301.660	66301.665	67728.816	67728.648	69123.664	69123.663	70484.296	70484.296	71810.861	71810.861
8	92055.319	87053.110	66326.238	66326.230	67753.123	67753.255	69147.591	69147.591	70507.864	70507.873	71834.067	71834.077
9	92089.403	87087.272	66353.897	66353.900	67780.432	67780.513	69174.504	69174.504	70534.378	70534.388	71860.180	71860.188
10	92127.273	87125.224	66384.639	66384.634	67810.788	67810.839	69204.407	69204.413	70563.834	70563.836	71889.180	71889.189
11	92168.921	87166.972	66418.438	66418.440	67844.167	67844.209	69237.299	69237.296	70596.226	70596.236	71921.079	71921.093
12	92214.350	87212.495	66455.330	66455.323	67880.575	67880.612	69273.175	69273.156	70631.561	70631.558	71955.868	71955.873
13	92263.561	87261.813	66495.280	66495.267	67919.992	67920.042	69312.017	69312.016	70669.816	70669.830	71993.544	71993.554
14	92316.544	87314.914	66538.300	66538.305	67962.454	67962.499	69353.848	69353.841	70711.020	70711.034	72034.102	72034.115
15	92373.300	87371.795	66584.391	66584.381	68007.923	68007.968	69398.653	69398.649	70755.147	70755.161	72077.551	72077.564
16	92433.829	87432.452	66633.546	66633.522	68056.394	68056.450	69446.422	69446.423	70802.202	70802.208	72123.885	72123.893
17	92498.128	87496.889	66685.753	66685.652	68107.913	68107.953	69497.171	69497.168	70852.185	70852.191	72173.094	72173.085
18	92566.198	87565.108	66740.992	66740.417	68162.407	68162.456	69550.873	69550.857	70905.086	70905.097	72225.167	72225.182
19	92638.026	87637.104	66799.255	66799.803	68219.900	68219.968	69607.503	69607.484	70960.910	70960.927	72280.107	72280.144
20	92713.617	87712.838	66860.352	66860.993	68280.389	68280.469	69667.176	69667.179	71019.655	71019.647	72337.941	72337.948
21	92792.967	87792.348	66927.043	66925.357	68343.852	68343.958	69729.750	69729.751	71081.294	71081.283	72398.616	72398.616
22	92876.077	87875.657	66993.251	66992.786	68410.260	68410.451	69795.297	69795.242	71145.844	71145.864	72462.156	72462.184
23	92962.941	87962.678	67063.585	67063.159	68479.559	68479.899	69863.749	69863.593	71213.330	71213.188	72528.577	72528.554
24	93053.559	88053.521	67137.064	67138.630	68551.373	68552.304	69935.138	69934.082	71283.672	71283.749	72597.782	72597.843
25	93147.920	88148.014	67213.596	67213.717		68627.604	70009.336	70010.255	71356.952	71356.958	72669.880	72669.840
26	93246.025	88246.282	67292.693	67292.699	68707.986	68705.698	70086.103	70087.264	71433.055	71433.070	72744.723	72744.649
27	93347.865	88348.285	67376.318	67376.227	68788.846	68786.116	70169.374	70167.337	71512.070	71512.063	72822.312[c]	
28	93453.457		67461.808	67461.748[c]	68872.906	68866.525	70251.109	70250.435[c]	71593.943	71593.998[c]	72903.043[c]	72901.288[c]
29	93562.765		67550.486	67550.365[c]	68960.079[c]	68963.120	70336.996[c]	70336.169[c]	71678.752[c]	71678.788[c]		72986.858[c]
30	93675.810		67642.094[c]	67642.030[c]	69050.105[c]	69052.123	70425.920[c]	70426.671[c]	71766.396[c]	71766.434[c]		73072.667[c]
31	93792.564		67736.801[c]	67736.683[c]	69142.454[c]	69144.909[c]	70517.765[c]	70517.946[c]	71856.892[c]	71856.936[c]		73163.250[c]
32	93913.047		67834.509[c]	67834.315[c]	69243.696[c]	69240.923[c]	70612.627[c]	70612.665[c]	71950.232[c]	71950.298[c]		73254.031[c]
33	94037.356		67935.175[c]	67934.877[c]	69340.595[c]	69339.953[c]	70709.931[c]	70709.934[c]	72046.262[c]	72046.497[c]		
34			68038.858[c]	68038.274[c]			70811.007[c]	70810.986[c]	72147.166[c]	72145.531[c]		
35				68148.228[c]			70914.511[c]	70914.501[c]				
								71020.875[c]				

[a] All values in cm^{-1}. [b] Level energies were calculated relative to the lowest $v = 0$ rovibrational level of the $X^1\Sigma^+$ ground state of $^{12}C^{17}O$ from the combined data sets of two experiments: the VUV-FTS study for the $C^1\Sigma^+$ ($v = 0$) and $B^1\Sigma^+$ ($v = 0$) levels, as well as VIS high-accuracy dispersive optical spectroscopy measurements for the $A^1\Pi$ ($v = 1$, 2, 3, 4, and 5) levels. The final values of the terms were obtained using the weighted average method. See Section 3.1 for details. [c] Level energies obtained by means of the deperturbed T_v rotation-less energies of $A^1\Pi$ (v) state from Table 10 and the relative terms of the $A^1\Pi$ (v) calculated on the basis of B–A[26,27] and C–A[28] bands by means of the least-squares method in the version given by Curl and Dane[78] and Watson.[79] The final values of the $A^1\Pi$ level energies are obtained using the weighted average method.

isotopologue. These data were combined with the B → A (this work, and ref. 26 and 27) as well as C → A[28] transition wavenumbers to give term values of the $A^1\Pi$ (v = 1, 2, 3, 4, and 5) levels as high as J_{max} = 27–30. They were calculated as differences of values of the $B^1\Sigma^+$ ($v = 0$), $C^1\Sigma^+$ ($v = 0$) terms and B → A ($0 - v''$), C → A ($0 - v''$) transition frequencies. A similar procedure was adopted to determine terms of the D, I, e, a′, and d perturbers in $^{12}C^{17}O$ using the $B^1\Sigma^+$ ($v = 0$) and $C^1\Sigma^+$ ($v = 0$) level energies and ($B^1\Sigma^+$, $C^1\Sigma^+$) → ($d^3\Delta_i$, $e^3\Sigma^-$, $a'^3\Sigma^+$, $I^1\Sigma^-$, and $D^1\Delta$) extra-lines (listed in Table 2). The $A^1\Pi$ (v) high-J level energies were calculated by means of the deperturbed T_v rotationless energies of the $A^1\Pi$ (v) state from Section 3.2 and relative terms of $A^1\Pi$ (v) calculated on the basis of B–A[26,27] and C–A[28] bands by means of the linear least-squares method in the version given by Curl and Dane[78] and Watson.[79] The final values of the $A^1\Pi$ energy levels are obtained using the weighted average method and are collected in Tables 5 and 6.

In order to display a visual presentation of perturbations occurring in the $^{12}C^{17}O$ $A^1\Pi$ (v = 1–5) rovibrational levels, we determined reduced term values $T(J) - B_A J(J+1) + D_A J^2(J+1)^2$ of the $A^1\Pi$ state with the hypothetical unperturbed and crossing perturber levels, where B_A and D_A refer to deperturbed rotational constants of the corresponding $A^1\Pi$ level. The reduced term values were calculated in relation to the lowest $v = 0$ rovibrational level of the $^{12}C^{17}O$ $X^1\Sigma^+$ ground state by means of the term values given in Tables 5 and 6. Those among the reduced terms which we were not able to determine from the experimental data, were calculated on the basis of isotopically recalculated equilibrium molecular constants by Field[30] for $d^3\Delta_i$, $e^3\Sigma^-$, $a'^3\Sigma^+$, and $I^1\Sigma^-$ states and by Kittrell *et al.*[81] for $D^1\Delta$ state. The T_e values were taken from ref. 81–83, and the $G(v = 0)$ value for the $X^1\Sigma^+$ state in $^{12}C^{17}O$, 1068.0310 cm^{-1}, from Coxon *et al.*[80] The results are presented in Fig. 6. Identification of perturbers for both e and f Λ-doubling components of the $A^1\Pi$ (v = 3, 4, and 5) levels are summarized in Table 7.

Table 6 Rovibronic term values of the $d^3\Delta_i$ ($v = 11$), $e^3\Sigma^-$ ($v = 4$), $a'^3\Sigma^+$ (v = 10, 13), $I^1\Sigma^-$ (v = 3, 6), and $D^1\Delta$ ($v = 1$) levels in $^{12}C^{17}O$[a]

State	v	J	Energy	Triplet component	Electronic symmetry
$e^3\Sigma^-$	4	25	68622.59	F_1	e
	4	26	68684.69	F_1	e
	4	25	68687.47	F_2	f
$a'^3\Sigma^+$	10	20	66875.28	F_2	e
	10	22	66923.16	F_1	f
	10	22	66971.69	F_2	e
	13	24	69942.13	F_1	f
	13	24	70047.62	F_3	f
	14	3	70296.10	F_2	e
$I^1\Sigma^-$	3	7	67730.78		f
	6	24	71269.82		f
$D^1\Delta$	1	26	67298.11		e
	1	27	67361.47		f

[a] All values in cm^{-1}. Level energies were calculated relative to the lowest $v = 0$ rovibrational level of the $X^1\Sigma^+$ ground state of $^{12}C^{17}O$ from the combined data sets of two experiments: the VUV-FTS study for the $C^1\Sigma^+$ ($v = 0$) and $B^1\Sigma^+$ ($v = 0$) levels, as well as VIS high-accuracy dispersive optical spectroscopy measurements for the $e^3\Sigma^-$ ($v = 4$), $a'^3\Sigma^+$ (v = 10, 13), $I^1\Sigma^-$ (v = 3, 6), and $D^1\Delta$ ($v = 1$) levels. The final values of the terms were obtained using the weighted average method.

3.2. Deperturbation analysis of the $A^1\Pi$ state in $^{12}C^{17}O$

In total, 982 transitions from 12 B–A, C–A, B–X, and C–X bands and their extra-lines of $^{12}C^{17}O$ were used in the global fitting procedure. This results in 72 molecular parameters fitted for this minor CO species. This analysis is performed, in analogy to deperturbation analyses of the main $^{12}C^{16}O$ isotopologue,[44,51] using the Pgopher software.[67] Applying this program we simulated each member of the B($v' = 0, 1$) − A(v'') and C($v' = 0$) − A(v'') progressions independently with a parameterised model of the A(v) levels, perturber levels, and their interactions. The computed level positions, line frequencies, and intensities are the result of a matrix diagonalization including all interacting levels. The assignment of perturber levels, the selection of which parameters and interactions could be discriminated from our spectra, and the values of these parameters were iteratively optimised. The Pgopher program[67] uses the effective Hamiltonian with matrix elements similar to Field,[30] Bergeman *et al.*,[84] and Le Floch *et al.*[31] The model is presented in Table 8. The non-diagonal elements describe the interaction of the $A^1\Pi$ state with its perturbers, that is the $d^3\Delta_i$, $e^3\Sigma^-$, $a'^3\Sigma^+$, $I^1\Sigma^-$, and $D^1\Delta$ states. Interactions between the perturbing states were neglected. For the $A^1\Pi$ diagonal element the '+' and '−' signs relating to Λ-doubling refer to the e- and f-symmetry states, respectively. T_v denotes the rotation-less energies calculated relative to the lowest rovibrational level of the $X^1\Sigma^+$ ground state, η_i is the spin–orbit interaction parameter, ξ_i is the L-uncoupling interaction parameter.

The $D^1\Delta$ and $d^3\Delta$ states have nearly degenerate e and f Λ-doublet components. The $e^3\Sigma^-$ state has two fine structure levels of e type and one f type, while the $a'^3\Sigma^+$ state has two fine structure levels of f type and one e type. By contrast, the $I^1\Sigma^-$ state has only f levels. The interactions between the $A^1\Pi$ state and the $e^3\Sigma^-$, $a'^3\Sigma^+$, and $d^3\Delta$ triplet states are caused by spin–orbit coupling, represented by J-independent matrix elements. Interactions of $A^1\Pi$ with the $I^1\Sigma^-$ and $D^1\Delta$ singlet states result from L-uncoupling and, therefore, produce heterogeneous interactions with J-dependent matrix elements.[32]

It was necessary to adopt some isotopically recalculated molecular constants, using Dunham's relationship within the Born–Oppenheimer approximation,[85] of $^{12}C^{16}O$ $d^3\Delta_i$, $e^3\Sigma^-$, $a'^3\Sigma^+$, $I^1\Sigma^-$, and $D^1\Delta$ states from ref. 30 and 81, because there are insufficient term-value data for these levels in $^{12}C^{17}O$ to determine these independently. These values were held fixed during the calculations. We only fitted molecular constants to those perturber states for which a sufficient number of transitions were observed in the present experiments. All possible vibrational levels of the perturbers which have a non-negligible influence on the $A^1\Pi$, v = 1, 2, 3, 4, and 5 levels were included in the calculation. Some of them do not have crossings with the $A^1\Pi$ state but still result in recognisable A-state energy level shifts.

The frequencies of strong and isolated lines were assigned relative weights of 1.0 during the fitting. However, the

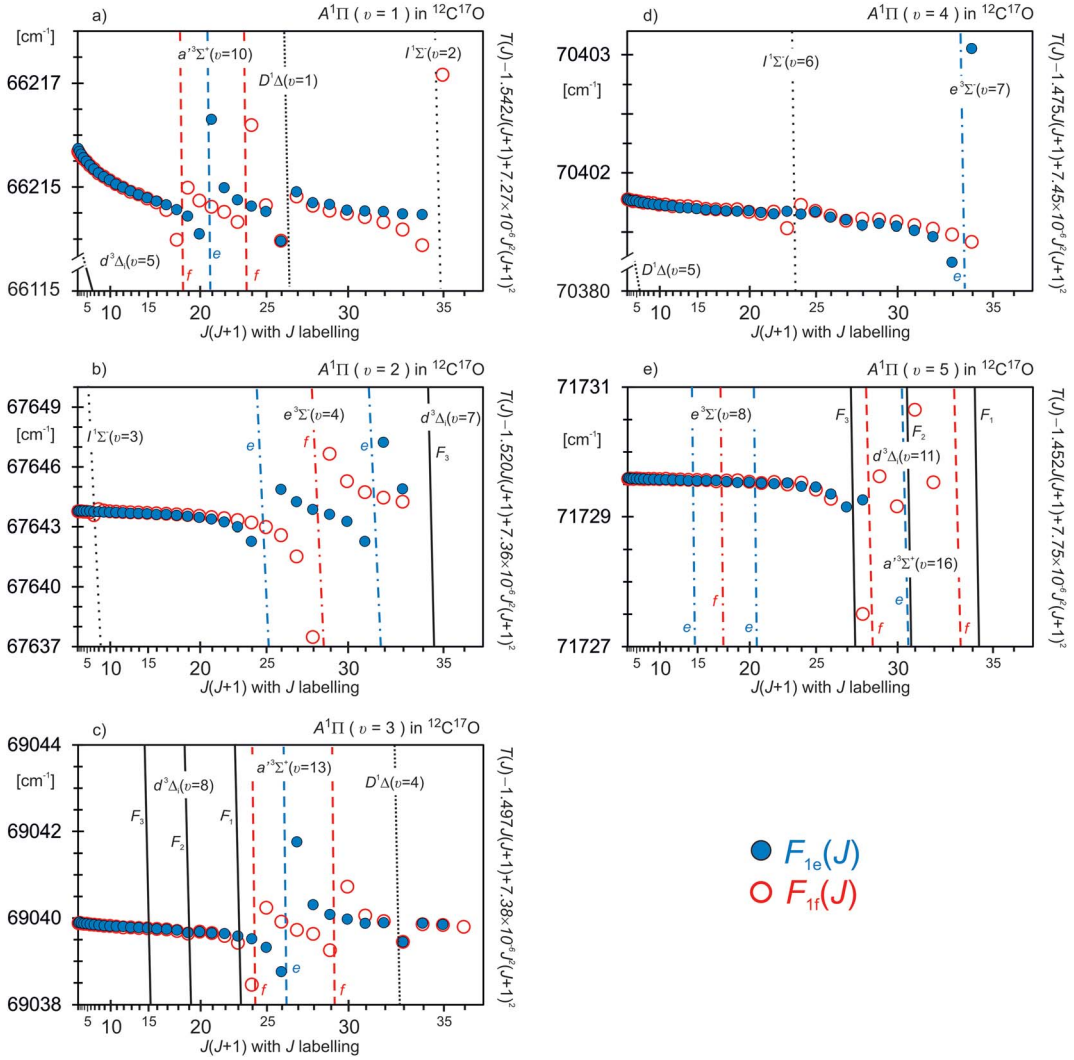

Fig. 6 The reduced $T(J) - B_A J(J+1) + D_A J^2(J+1)^2$ term values for the $^{12}C^{17}O$ $A^1\Pi$ ($\upsilon = 1$–5) levels and for the hypothetical unperturbed crossing rovibronic levels of the perturbers. Filled and open circles indicate e and f electronic symmetry of the $A^1\Pi$ state, respectively. The reduced level energies (in cm^{-1}) were calculated in relation to the lowest $\upsilon = 0$ rovibrational level of the $X^1\Sigma^+$ ground state by means of terms calculated in this work (see Tables 5 and 6). Some reduced terms were calculated on the basis of isotopically recalculated equilibrium molecular constants given by Field[30] for $d^3\Delta_i$, $e^3\Sigma^-$, $a'^3\Sigma^+$, and $l^1\Sigma^-$ states and by Kittrell *et al.*[81] for $D^1\Delta$ state. The T_e values were taken from ref. 81–83, and the $G(\upsilon = 0)$ value for the $X^1\Sigma^+$ state in $^{12}C^{17}O$, 1068.0310 cm^{-1}, from Coxon *et al.*[80] B_A and D_A symbols refer to deperturbed rotational constants of the respective $A^1\Pi$ rovibronic level, determined in this work (see Table 10). Note that different reduced-energy scales in cm^{-1} are used for different vibrational levels of $A^1\Pi$.

frequencies of weak and/or blended lines have lower accuracy, so they were individually weighted between 0.5 and 0.1, according to the degree of their weakening and/or overlap.

Initial fits were made by varying the B, D, H rotational constants and the q Λ-doubling constant of the $A^1\Pi$ ($\upsilon = 1$–5) levels. This means that all parity-dependent interactions were included explicitly in the interactions contained in our deperturbation. Any additional Λ-doubling from remote perturbers was aliased by the interactions included in our perturbation. During the deperturbation, the rotational B and D parameters of the $X^1\Sigma^+$ ($\upsilon = 0$) ground state were fixed to the values given by Coxon[80] for $^{12}C^{17}O$.

The unweighted *obs-calc* residuals of the fitting method are dominated by the uncertainties of the very weak and heavily perturbed lines that belong to the weakest B–A (1, 1) and (1, 5) bands. The weighted contribution to the root-mean-square (rms) residual value of high-accuracy dispersive optical spectroscopy and VUV-FTS data is 0.006 cm^{-1}. This shows that the fitting model acceptably reproduces such a comprehensive experimental data set.

In a few cases, fitting of the interaction parameters was statistically unjustified because there was an insufficient quantity of experimental transitions in the vicinity of the avoided crossings of the perturbing states or because of the interaction of energetically remote states (for $J < 0$ or $J > J_{max}$) without any observed crossing points with the $A^1\Pi$ state in $^{12}C^{17}O$. In such cases we estimated the semi-empirical interaction parameters making use of the quality suggested in ref. 31, 41

Table 7 Observed and predicted perturbations in the $A^1\Pi$, $v = 3$, 4, and 5 rovibrational levels of the $^{12}C^{17}O$ isotopologue[a]

	Perturbing state		J value for the maximum of perturbation in Λ-doubling components			
			f		e	
Perturbed state	Vibrational level	Triplet component	Observed	Calculated	Observed	Calculated
$A^1\Pi$ ($v = 3$)	$e^3\Sigma^-$ ($v = 5$)	F(1)			[b]	<1
		F(2)	[b]	<1		
		F(3)			[b]	<1
	$d^3\Delta_i$ ($v = 8$)	F(3)	Negligibly small[c]	15–16	Negligibly small[c]	15–16
		F(2)	19–20 (very weak)[c]	19–20	19–20 (very weak)[c]	19–20
		F(1)	[d]	23–24	[d]	23–24
	$a'^3\Sigma^+$ ($v = 13$)	F(1)	24–25	23–24		
		F(2)			**26–27**	26–27
		F(3)	29–**30**	29–30		
	$D^1\Delta$ ($v = 4$)		**33** (weak)[c]	33	**33** (weak)[c]	33
	$I^1\Sigma^-$ ($v = 5$)		[b]	40–41		
$A^1\Pi$ ($v = 4$)	$a'^3\Sigma^+$ ($v = 14$)	F(1)	[b]	<1		
		F(2)			**<1**	<1
		F(3)	**<1**	<1		
	$D^1\Delta$ ($v = 5$)		**<1**	<1	**<1**	<1
	$I^1\Sigma^-$ ($v = 6$)		**23–24**	23		
	$e^3\Sigma^-$ ($v = 7$)	F(1)			**33–34**	34
		F(2)	[b]	37		
		F(3)			[b]	40
	$a'^3\Sigma^+$ ($v = 15$)	F(1)	[b]	40–41		
		F(2)			[b]	43–44
		F(3)	[b]	46–47		
	$d^3\Delta_i$ ($v = 10$)	F(3)	[b]	40	[b]	40
		F(2)	[b]	44	[b]	44
		F(1)	[b]	48	[b]	48
$A^1\Pi$ ($v = 5$)	$e^3\Sigma^-$ ($v = 8$)	F(1)			14 (very weak)[c]	14
		F(2)	17 (very weak)[c]	17		
		F(3)			**20** (very weak)[c]	20
	$d^3\Delta_i$ ($v = 11$)	F(3)	[e]	26–27	[f]	26–27
		F(2)	[e]	30–31	[b]	30–31
		F(1)	[b]	34–35	[b]	34–35
	$a'^3\Sigma^+$ ($v = 16$)	F(1)	**28–29**	27–28		
		F(2)			**30–31**	30–31
		F(3)	[b]	33–34		
	$D^1\Delta$ ($v = 7$)		[b]	37	[b]	37

[a] The values in bold correspond to perturbations observed for the first time in $^{12}C^{17}O$. [b] Theoretically predicted interaction of energetically remote states (for $J < 0$ or $J > J_{max}$) without any observed crossing points with the $A^1\Pi$ state but the deperturbation fit shows that they have a noticeable influence on the $A^1\Pi$ ($v = 3$, 4, or 5) levels (see Table 10). [c] See Table 10. [d] Perturbation difficult to identify on the basis of observations only (*e.g.* Fig. 6) due to much stronger interaction that exists in this region due to the $a'^3\Sigma^+$ ($v = 13$) state. Its significance can be evaluated only on the basis of results of deperturbation fit provided in Table 10. [e] Perturbation difficult to identify on the basis of observations only (*e.g.* Fig. 6) due to stronger interaction that exists in this region deriving from the F_1 term of the $a'^3\Sigma^+$ ($v = 16$) state. Its significance can be evaluated only on the basis of results of deperturbation fit provided in Table 10. [f] Perturbation difficult to identify on the basis of observations only (*e.g.* Fig. 6) because of uncharacteristic behaviour of the rovibrational e-parity terms at $J = 26$–28 due to overlapping interaction with distant a substantially interaction with the F_2 term of the $a'^3\Sigma^+$ ($v = 16$) state.

and 88, which shows that for perturbation between vibronic levels of a given pair of electronic states, the perturbation matrix element (α, β) is the product of a vibrational factor and a constant electronic perturbation parameter ($\boldsymbol{a}$, $\boldsymbol{b}$). The effective perturbation parameters α and β, in the e/f basis set, are defined as follows:

$$\alpha_{A\sim d} = \langle A^1\Pi,\ v_A\ |\boldsymbol{H}^{SO}|\ d^3\Delta,\ v_d\rangle = -\left(\frac{\sqrt{2}}{4}\right)\boldsymbol{a}_{\mathbf{A}\sim\mathbf{d}}\langle v_A|v_d\rangle, \quad (1)$$

$$\alpha_{A\sim e} = \langle A^1\Pi,\ v_A\ |\boldsymbol{H}^{SO}|e^3\Sigma^-,\ v_e\rangle = -\left(\frac{1}{4}\right)\boldsymbol{a}_{\mathbf{A}\sim\mathbf{e}}\langle v_A|v_e\rangle, \quad (2)$$

$$\alpha_{A\sim a'} = \left\langle A^1\Pi,\ v_A\ |\boldsymbol{H}^{SO}|a'^3\Sigma^+,\ v_{a'}\right\rangle = \left(\frac{1}{4}\right)\boldsymbol{a}_{\mathbf{A}\sim\mathbf{a}'}\langle v_A|v_{a'}\rangle, \quad (3)$$

$$2\beta_{A\sim I}\sqrt{J(J+1)} = \langle A^1\Pi,\ v_A\ |\boldsymbol{H}^{RE}|I^1\Sigma^-,\ v_I\rangle = -\sqrt{J(J+1)}\ \boldsymbol{b}_{\mathbf{A}\sim\mathbf{I}}\ \langle v_A|\boldsymbol{B}(\boldsymbol{R})|v_I\rangle, \quad (4)$$

$$\beta_{A\sim D}\sqrt{J(J+1)-2} = \langle A^1\Pi,\ v_A\ |\boldsymbol{H}^{RE}|D^1\Delta,\ v_D\rangle = \sqrt{J(J+1)-2}\ \boldsymbol{b}_{\mathbf{A}\sim\mathbf{D}}\ \langle v_A|\boldsymbol{B}(\boldsymbol{R})|v_D\rangle, \quad (5)$$

where $\boldsymbol{H}^{SO}$ and $\boldsymbol{H}^{RE}$ are the spin–orbit and rotation-electronic operators, respectively, and $\boldsymbol{a} = \langle 2\pi|a\boldsymbol{l}^+|2\sigma\rangle$, $\boldsymbol{b} = \langle 2\pi|\boldsymbol{l}^+|2\sigma\rangle$. It

Table 8 Effective Hamiltonian and matrix elements for perturbation analyses of the $A^1\Pi$ ($v = 1$, 2, 3, 4, and 5) rovibronic levels and their perturbers in $^{12}C^{17}O$[a,b,c]

	$A^1\Pi$	$I^1\Sigma^-$	$D^1\Delta$	$e^3\Sigma^-$	$a'^3\Sigma^+$	$d^3\Delta_i$
$A^1\Pi$	$T_v + \left(B \pm \frac{q}{2}\right)\hat{N}^2 - D\hat{N}^4 + H\hat{N}^6$	$\xi_i(I_v) \times (\hat{N}_+\hat{L}_- + \hat{N}_-\hat{L}_+)$	$\xi_i(D_v) \times (\hat{N}_+\hat{L}_- + \hat{N}_-\hat{L}_+)$	$\eta_i(e_v)\hat{L}\cdot\hat{S}$	$\eta_i(a'_v)\hat{L}\cdot\hat{S}$	$\eta_i(d_v)\hat{L}\cdot\hat{S}$
$I^1\Sigma^-$		$T_v + B\hat{N}^2 - D\hat{N}^4 + H\hat{N}^6$	0	0	0	0
$D^1\Delta$			$T_v + B\hat{N}^2 - D\hat{N}^4 + H\hat{N}^6$	0	0	0
$e^3\Sigma^-$				$T_v + B\hat{N}^2 - D\hat{N}^4 + H\hat{N}^6 + \frac{2}{3}\lambda(3\hat{S}_z{}^2 - \hat{S}^2)$	0	0
$a'^3\Sigma^+$					$T_v + B\hat{N}^2 - D\hat{N}^4 + H\hat{N}^6 + \frac{2}{3}\lambda\left(3\hat{S}_z{}^2 - \hat{S}^2\right) + \gamma(\hat{N}\cdot\hat{S})$	
$d^3\Delta_i$						$T_v + B\hat{N}^2 - D\hat{N}^4 + H\hat{N}^6 + \frac{2}{3}\lambda(3\hat{S}_z{}^2 - \hat{S}^2) + \gamma(\hat{N}\cdot\hat{S}) + A\hat{L}_z\hat{S}_z + \frac{1}{2}A_D\lambda(\hat{N}^2\hat{L}_z\hat{S}_z + \hat{L}_z\hat{S}_z\hat{N}^2)$

[a] The model is consistent with that of Pgopher software.[67] [b] The matrix is symmetric, therefore, the lower left non-diagonal elements, which are not shown in the Hamiltonian, are equivalent to those of the corresponding upper right elements. The matrix elements set to zero are results of an approximation consisting in neglecting the mutual interaction between the perturbing states. For the $A^1\Pi$ diagonal element the '+' and '−' signs relating to Λ-doubling refer to the e- and f-symmetry states, respectively. [c] T_v – denotes the rotation-less energies calculated relative to the lowest rovibrational level of the $X^1\Sigma^+$ ground state, η_i – spin–orbit interaction parameter, ξ_i – *L*-uncoupling interaction parameter. The rest of the parameters used are defined in the open literature.[68,86,87]

Table 9 Perturbation parameters of the $A^1\Pi\sim(d^3\Delta_i, e^3\Sigma^-, a'^3\Sigma^+, I^1\Sigma^-$, and $D^1\Delta$) interactions, fixed in the $^{12}C^{17}O$ deperturbation analysis

Interaction	$\boldsymbol{a}^a$ (cm^{-1})	$\langle v_A\|v_{pert}\rangle^b$	η^c (cm^{-1})
$A^1\Pi$ ($v=3$)$\sim d^3\Delta$ ($v=8$)	95.3	−0.0026	0.15
$A^1\Pi$ ($v=4$)$\sim d^3\Delta$ ($v=10$)	95.3	−0.0295	1.72
$A^1\Pi$ ($v=1$)$\sim e^3\Sigma^-$ ($v=3$)	98.9	−0.0964	4.13
$A^1\Pi$ ($v=3$)$\sim e^3\Sigma^-$ ($v=5$)	98.9	−0.2061	8.83
$A^1\Pi$ ($v=5$)$\sim e^3\Sigma^-$ ($v=8$)	98.9	0.0001	-0.58×10^{-2}
$A^1\Pi$ ($v=2$)$\sim a'^3\Sigma^+$ ($v=11$)	83.4	−0.1937	−6.99
$A^1\Pi$ ($v=2$)$\sim a'^3\Sigma^+$ ($v=12$)	83.4	0.1565	5.65
$A^1\Pi$ ($v=4$)$\sim a'^3\Sigma^+$ ($v=15$)	83.4	−0.1931	−6.97

Interaction	b^a (unitless)	$\langle v_A\|\boldsymbol{B}\|v_{pert}\rangle^b$ (cm^{-1})	ξ^c (cm^{-1})
$A^1\Pi$ ($v=3$)$\sim I^1\Sigma^-$ ($v=5$)	0.227	−0.2023	3.25×10^{-2}
$A^1\Pi$ ($v=5$)$\sim I^1\Sigma^-$ ($v=8$)	0.227	−0.1230	1.98×10^{-2}
$A^1\Pi$ ($v=2$)$\sim D^1\Delta$ ($v=2$)	0.11	0.0381	4.19×10^{-3}
$A^1\Pi$ ($v=4$)$\sim D^1\Delta$ ($v=5$)	0.11	−0.3523	-3.88×10^{-2}
$A^1\Pi$ ($v=5$)$\sim D^1\Delta$ ($v=7$)	0.11	0.3203	3.52×10^{-2}

[a] The spin–orbit and rotation-electronic perturbation parameters $\boldsymbol{a}$ and $\boldsymbol{b}$ were taken from Le Floch *et al.*[31] (Table 2). [b] The vibrational integrals were calculated on the basis of $^{12}C^{17}O$ RKRs of A, d, e, a′, I, and D states obtained from isotopically recalculated equilibrium constants of Field,[30] Field *et al.*,[32,87] Le Floch *et al.*,[31] and Kittrell *et al.*[81] and using the computer programs 'LEVEL' of Le Roy[89] as well as 'FRACON' of Jung[90] (later modified by Jakubek[91]). See Section 3.2 for details. [c] The perturbation parameters, fixed during the $^{12}C^{17}O$ deperturbation fits. They were calculated on the basis of eqn (1)–(8) using electronic perturbation parameters and vibrational integrals given in the current table.

is then possible to calculate initial values of interaction parameters for any pair of levels whenever the relevant vibrational wavefunctions are known.[31] So, the missing perturbation parameters, which were fixed during the deperturbation calculation, were estimated on the basis of the isotopologue-independent purely electronic perturbation parameters $\boldsymbol{a}$ and $\boldsymbol{b}$ of Le Floch,[31] as well as $\langle v_A|v_{d,e,or\ a'}\rangle$ vibrational overlap integrals and the $\langle v_A|\boldsymbol{B}(\boldsymbol{R})|v_{I\ or\ D}\rangle$ rotational operator integral in $^{12}C^{17}O$, according to eqn (1)–(8). These parameters are presented in Table 9. The vibrational integrals were calculated on the basis of $^{12}C^{17}O$ RKRs of A, d, e, a′, I, and D states obtained from isotopically recalculated equilibrium constants of Field,[30] Field *et al.*,[32,87] Le Floch *et al.*,[31] and Kittrell *et al.*[81] and using the computer programs 'LEVEL' of Le Roy[89] as well as 'FRACON' of Jung[90] (later modified by Jakubek[91]). Then, justification of the use of each of those estimated values in the fit was tested. Only those were used that led to noticeable improvements in the quality of the fit within the accuracy obtained.

A careful examination of the correlation matrix shows satisfactorily low correlations between fitted model parameters. The final set of deperturbed molecular constants from the fits is presented mainly in Tables 10 and 11. The relationships between the η and α as well as ξ and β perturbation parameters result from their different definitions,[30,67,94,95] which affect the interaction matrix elements, are as follows:

$$\eta_i = \alpha_i\sqrt{3}\ , \tag{6}$$

$$\xi_{A\sim I} = \beta_{A\sim I}\sqrt{2}, \tag{7}$$

$$\xi_{A\sim D} = \beta_{A\sim D}, \tag{8}$$

where subscript 'i' indicates A∼d, A∼e, as well as A∼a′ interactions.

The spin–orbit and rotation-electronic parameters obtained from the $^{12}C^{17}O$ $A^1\Pi$ (v = 1–5) deperturbation analysis are collected in Table 11. The isotopologue independent, electronic perturbation parameters $\boldsymbol{a}$ and $\boldsymbol{b}$ for the $A^1\Pi\sim(d^3\Delta_i, e^3\Sigma^-, a'^3\Sigma^+, I^1\Sigma^-$, and $D^1\Delta$) interactions are in very good agreement with the values given by Le Floch[31] (see Table 9) Field,[30] and Field *et al.*[32,87]

While performing the deperturbation calculations, we also obtained the rovibrational constants for the $B^1\Sigma^+$ (v = 0 and 1) and $C^1\Sigma^+$ (v = 0) Rydberg states in $^{12}C^{17}O$. The results are given in Table 12. The constants for the $B^1\Sigma^+$ and $C^1\Sigma^+$ states are compared with analogous values derived in previous studies.[26–28]

3.3. Equilibrium constants and transition probabilities in $^{12}C^{17}O$

Equilibrium constants of the $A^1\Pi$ state in $^{12}C^{17}O$ were determined on the basis of the $A^1\Pi$ (v = 1–5) deperturbed constants summarised in Table 10, using a weighted least-squares method. The results are collected in Table 13 and expressed as Dunham coefficients. Despite the fact that Dunham parameters do not include the parameters that describe perturbations between the zero-order states and they are not expected to fit the data to measurement accuracy, they are the most appropriate input to RKR and Franck–Condon Factors (FCF) calculations. It allowed for obtaining the FCF for the Ångström ($B^1\Sigma^+$–$A^1\Pi$), Herzberg ($C^1\Sigma^+$–$A^1\Pi$) and Fourth positive ($A^1\Pi$–$X^1\Sigma^+$) systems using the deperturbed RKR potential energy curve parameters of the $^{12}C^{17}O$ $A^1\Pi$ (this work), $B^1\Sigma^+$ (ref. 27), $C^1\Sigma^+$ (ref. 28), and $X^1\Sigma^+$ (ref. 80) states. The FCFs in $^{12}C^{17}O$ are provided in Table 14.

4. Discussion

Fig. 6a–e show plots of the $^{12}C^{17}O$ $A^1\Pi$, v = 1–5 reduced term values together with a diabatic representation of the perturbers. The strongest perturbations occur because of the spin–orbit interactions with the $d^3\Delta_i$, $a'^3\Sigma^+$, and $e^3\Sigma^-$ triplet states. They lead to clearly visible splitting of the Λ-doublet components in regions of avoiding crossings. This phenomenon is most visible for $A^1\Pi$ (v = 1) at J = 18–24 caused by $a'^3\Sigma^+$ (v = 10) with term shifts of ∼2.5 cm^{-1}, $A^1\Pi$ (v = 2) at J = 25–32 caused by $e^3\Sigma^-$ (v = 4) with maximum term shifts of ∼4 cm^{-1}, $A^1\Pi$ (v = 3) at J = 24–30 caused by $a'^3\Sigma^+$ (v = 13) with maximum term shifts of ∼3 cm^{-1}, and for $A^1\Pi$ (v = 5) where we observe a complex perturbation pattern occurring at J = 28–32 resulting from the interactions with the three spin components of $d^3\Delta_i$ (v = 11) and $a'^3\Sigma^+$ (v = 16) with maximum term shifts of about 2.5 cm^{-1}. In

Table 10 Deperturbed molecular constants (in cm^{-1}) of the $A^1\Pi$, $v = 1$, 2, 3, 4, and 5 rovibronic levels and their perturbers in $^{12}C^{17}O$[a]

Constant/level	$A^1\Pi$ ($v = 1$)	$A^1\Pi$ ($v = 2$)	$A^1\Pi$ ($v = 3$)	$A^1\Pi$ ($v = 4$)	$A^1\Pi$ ($v = 5$)
T_v	66214.2529 (87)	67643.9829 (31)	69039.7043 (16)	70401.6687 (63)	71729.6882 (17)
B_v	1.541 758 (21)	1.519 578 (11)	1.497 130 4 (92)	1.474 504 (15)	1.451 844 (11)
$D_v \times 10^6$	7.275 (16)	7.361 (11)	7.383 (10)	7.447 (13)	7.754 (15)
$H_v \times 10^{11}$	−1.26[b]	−1.26[b]	−1.26[b]	−1.26[b]	−1.26[b]
Constant/level	$d^3\Delta_i$ ($v = 5$)	$d^3\Delta_i$ ($v = 7$)	$d^3\Delta_i$ ($v = 8$)	$d^3\Delta_i$ ($v = 10$)	$d^3\Delta_i$ ($v = 11$)
T_v	66117.62[c]	68178.22[c]	69180.76[c]	71131.06[c]	72079.01[c]
B_v	1.186 79[d]	1.154 46[d]	1.138 55[d]	1.107 25[d]	1.091 82[d]
A_v	−16.523[d]	−16.830[d]	−16.984[d]	−17.291[d]	−17.444[d]
λ_v	0.898[e]	1.094[e]	1.191[e]	1.387[e]	1.485[e]
$\gamma_v \times 10^3$	−8.13[f]	−8.13[f]	−8.13[f]	−8.13[f]	−8.13[f]
$D_v \times 10^6$	6.13[d]	6.10[d]	6.09[d]	6.08[d]	6.08[d]
$H_v \times 10^{13}$	−7.41[g]	−7.41[g]	−7.41[g]	−7.41[g]	−7.41[g]
$A_{Dv} \times 10^5$	−4.94[f]	−4.94[f]	−4.94[f]	−4.94[f]	−4.94[f]
η	−16.455 (54)	10.21 (19)	0.15[h]	1.72[h]	7.915 (44)
Constant/level	$e^3\Sigma^-$ ($v = 3$)	$e^3\Sigma^-$ ($v = 4$)	$e^3\Sigma^-$ ($v = 5$)	$e^3\Sigma^-$ ($v = 7$)	$e^3\Sigma^-$ ($v = 8$)
T_v	66900.71[i]	67924.973 (35)	68930.84[i]	70886.156 (13)	71836.97[i]
B_v	1.191 69[d]	1.175 145 (46)	1.158 79[d]	1.126 417[d]	1.110 34[d]
λ_v	0.542[e]	0.557 (11)	0.576[e]	0.611[e]	0.628[e]
$D_v \times 10^6$	6.39[d]	6.35[d]	6.33[d]	6.29[d]	6.28[d]
$H_v \times 10^{12}$	−1.85[g]	−1.85[g]	−1.85[g]	−1.85[g]	−1.85[g]
η	4.13[h]	12.981 (79)	8.83[h]	−6.792 (27)	−0.0058[h]
Constant/level	$a'^3\Sigma^+$ ($v = 10$)	$a'^3\Sigma^+$ ($v = 11$)	$a'^3\Sigma^+$ ($v = 13$)	$a'^3\Sigma^+$ ($v = 14$)	$a'^3\Sigma^+$ ($v = 16$)
T_v	66398.5691 (51)	67397.25[i]	69339.963 (17)	70284.08[i]	72118.33[i]
B_v	1.137 90[d]	1.122 35[d]	1.091 481 (23)	1.076 07[d]	1.045 37[d]
λ_v	−1.131 4 (86)	−1.126[e]	−1.114 1 (75)	−1.106[e]	−1.092[e]
$\gamma_v \times 10^3$	−5.85 (34)	−6.27[f]	−6.19 (24)	−6.27[f]	−6.27[f]
$D_v \times 10^6$	5.95[d]	5.94[d]	5.93[d]	5.93[d]	5.92[d]
$H_v \times 10^{13}$	−3.7[g]	−3.7[g]	−3.7[g]	−3.7[g]	−3.7[g]
η	−4.918 (73)	−6.99[h]	7.091 (11)	7.63 (15)	−6.803 (31)
Constant/level		$a'^3\Sigma^+$ ($v = 12$)		$a'^3\Sigma^+$ ($v = 15$)	
T_v		68377.68[i]		71210.21[i]	
B_v		1.106 87[d]		1.060 72[d]	
λ_v		−1.119[e]		−1.099[e]	
$\gamma_v \times 10^3$		−6.27[f]		−6.27[f]	
$D_v \times 10^6$		5.94[d]		5.92[d]	
$H_v \times 10^{13}$		−3.7[g]		−3.7[g]	
η		5.65[h]		−6.97[h]	
Constant/level	$I^1\Sigma^-$ ($v = 2$)	$I^1\Sigma^-$ ($v = 3$)	$I^1\Sigma^-$ ($v = 5$)	$I^1\Sigma^-$ ($v = 6$)	$I^1\Sigma^-$ ($v = 8$)
T_v	66647.75[j]	67664.68[j]	69639.21[j]	70596.1599 (73)	72454.96[j]
B_v	1.195 01[d]	1.177 87[d]	1.143 67[d]	1.126 67[d]	1.092 91[d]
$D_v \times 10^6$	6.54[g]	6.56[g]	6.60[g]	6.62[g]	6.66[g]
$H_v \times 10^{12}$	2.78[g]	2.78[g]	2.78[g]	2.78[g]	2.78[g]
$\xi \times 10^2$	−7.420 (15)	−5.75 (10)	3.25[h]	−1.76 (11)	1.98[h]
Constant/level	$D^1\Delta$ ($v = 1$)	$D^1\Delta$ ($v = 2$)	$D^1\Delta$ ($v = 4$)	$D^1\Delta$ ($v = 5$)	$D^1\Delta$ ($v = 7$)
T_v	66458.5762 (48)	67468.27[l]	69429.99[l]	70382.01[l]	72228.37[l]
B_v	1.199 71[k]	1.182 76[k]	1.148 86[k]	1.131 91[k]	1.098 01[k]

Table 10 (*Contd.*)

Constant/level	$D^1\Delta$ ($v = 1$)	$D^1\Delta$ ($v = 2$)	$D^1\Delta$ ($v = 4$)	$D^1\Delta$ ($v = 5$)	$D^1\Delta$ ($v = 7$)
$D_v \times 10^6$	6.69[k]	6.65[k]	6.62[k]	6.60[k]	6.56[k]
$H_v \times 10^{13}$	−2.78[g]	−2.78[g]	−2.78[g]	−2.78[g]	−2.78[g]
$\xi \times 10^2$	−6.64 (23)	0.42[h]	−1.68 (23)	−3.88[h]	3.52[h]

[a] The parameters without indicating uncertainties are taken from the literature and held fixed during the fitting. T_v denotes the energy level separations between the ground state $X^1\Sigma^+$ ($v = 0, J = 0$) and excited state ($v = 0, J = 0$) of $^{12}C^{17}O$, η_i – spin–orbit interaction parameter, and ξ_i – *L*-uncoupling interaction parameter. [b] Isotopically recalculated from Le Floch.[42] [c] Calculated on the basis of isotopically recalculated vibrational equilibrium constants of $d^3\Delta_i$ by Field,[30] $X^1\Sigma^+$ by Le Floch[92] and T_e of $d^3\Delta_i$ from Huber and Herzberg.[83] [d] Isotopically recalculated from Field.[30] [e] Isotopically recalculated from spin–spin *C* constants of Field[30] taking into account the equation $\lambda = -\left(\frac{3}{2}\right)C$ (see Table 3.4 in ref. 87). [f] Calculated on the basis of Field's data[30] using the conversion 29979, 2458 MHz cm^{-1},[92] isotopically recalculated to $^{12}C^{17}O$. [g] Isotopically recalculated from Le Floch.[31] [h] Estimated on the basis of the isotopologue-independent purely electronic perturbation parameters $\boldsymbol{a}$ and $\boldsymbol{b}$ of Field[32,41] and Le Floch,[31] as well as $\langle v_A|v_{d,e\ or\ a'}\rangle$ and $\langle v_A|B|v_{I\ or\ D}\rangle$ in $^{12}C^{17}O$ from Table 9, according to the eqn (1)–(8). See Section 3.2 for details. [i] Calculated on the basis of isotopically recalculated vibrational equilibrium constants of $a'^3\Sigma^+$ by Field,[30] $X^1\Sigma^+$ by Le Floch[92] and T_e of the perturber by Tilford *et al.*[82] [j] Calculated on the basis of isotopically recalculated vibrational equilibrium constants of $I^1\Sigma^-$ by Field,[30] $X^1\Sigma^+$ by Le Floch[92] and T_e of $I^1\Sigma^-$ from Herzberg *et al.*[93] [k] Isotopically recalculated from Kittrell *et al.*[81] [l] Calculated on the basis of isotopically recalculated vibrational equilibrium constants of $D^1\Delta$ by Kittrell *et al.*,[81] $X^1\Sigma^+$ by Le Floch[92] and T_e of $D^1\Delta$ by Kittrell *et al.*[81]

Table 11 Spin–orbit and rotation-electronic parameters obtained from deperturbation analysis of the $A^1\Pi$, $v = 1$–5 levels in $^{12}C^{17}O$[a]

Interaction	$\langle v_A\|v_{pert}\rangle$[b]	η (cm^{-1})	$\eta/\langle v_A\|v_{pert}\rangle$ (cm^{-1})	$\boldsymbol{a}$[c] (cm^{-1})	$\bar{\boldsymbol{a}}$[d] (cm^{-1})
$A^1\Pi$ ($v = 1$)~$d^3\Delta$ ($v = 5$)	0.2803	−16.455 (54)	−58.71 (19)	95.87 (31)	95.59 (27)
$A^1\Pi$ ($v = 2$)~$d^3\Delta$ ($v = 7$)	−0.1763	10.21 (19)	−57.9 (11)	94.6 (18)	
$A^1\Pi$ ($v = 5$)~$d^3\Delta$ ($v = 11$)	−0.1362	7.915 (44)	−58.12 (32)	94.90 (53)	
$A^1\Pi$ ($v = 2$)~$e^3\Sigma^-$ ($v = 4$)	−0.2967	12.981 (79)	−43.76 (27)	101.05 (61)	98.90 (33)
$A^1\Pi$ ($v = 4$)~$e^3\Sigma^-$ ($v = 7$)	0.1600	−6.792 (27)	−42.46 (17)	98.05 (39)	
$A^1\Pi$ ($v = 1$)~$a'^3\Sigma^+$ ($v = 10$)	−0.1371	−4.918 (73)	35.87 (53)	82.9 (12)	83.62 (12)
$A^1\Pi$ ($v = 3$)~$a'^3\Sigma^+$ ($v = 13$)	0.1957	7.091 (11)	36.226 (56)	83.66 (13)	
$A^1\Pi$ ($v = 4$)~$a'^3\Sigma^+$ ($v = 14$)	0.2098	7.63 (15)	36.36 (72)	84.0 (17)	
$A^1\Pi$ ($v = 5$)~$a'^3\Sigma^+$ ($v = 16$)	−0.1883	−6.803 (31)	36.12 (16)	83.42 (38)	

Interaction	$\langle v_A\|\boldsymbol{B}\|v_{pert}\rangle$[b] ($cm^{-1}$)	$\xi \times 10^2$ (cm^{-1})	$\xi/\langle v_A\|\boldsymbol{B}\|v_{pert}\rangle$ (unitless)	$\boldsymbol{b}$[c] (unitless)	$\bar{\boldsymbol{b}}$[d] (unitless)
$A^1\Pi$ ($v = 1$)~$I^1\Sigma^-$ ($v = 2$)	0.4618	−7.420 (15)	−0.16067 (33)	0.22722 (46)	0.2274 (46)
$A^1\Pi$ ($v = 2$)~$I^1\Sigma^-$ ($v = 3$)	0.3412	−5.75 (10)	−0.1685 (31)	0.2384 (43)	
$A^1\Pi$ ($v = 4$)~$I^1\Sigma^-$ ($v = 6$)	0.1065	−1.76 (11)	−0.165 (10)	0.234 (15)	
$A^1\Pi$ ($v = 1$)~$D^1\Delta$ ($v = 1$)	−0.5818	−6.64 (23)	0.1142 (40)	0.1142 (40)	0.1103 (14)
$A^1\Pi$ ($v = 3$)~$D^1\Delta$ ($v = 4$)	−0.1534	−1.68 (23)	0.1098 (15)	0.1098 (15)	

[a] Uncertainties in parentheses correspond to one standard deviation. [b] The vibrational integrals were calculated on the basis of $^{12}C^{17}O$ RKRs of A, d, e, a′, I, and D states obtained from isotopically recalculated equilibrium constants of Field,[30] Field *et al.*,[32,87] Le Floch *et al.*,[31] and Kittrell *et al.*[81] and using the computer programs 'LEVEL' of Le Roy[89] as well as 'FRACON' of Jung[90] (later modified by Jakubek[91]). [c] The spin–orbit and rotation-electronic perturbation parameters $\boldsymbol{a}$ and $\boldsymbol{b}$ were calculated on the basis of eqn (1)–(8). [d] The weighted average values of the electronic perturbation parameters obtained in this work.

Table 12 Molecular constants of the $B^1\Sigma^+$ ($v = 0$, 1) and $C^1\Sigma^+$ ($v = 0$) Rydberg states in $^{12}C^{17}O$[a,b]

Level/constant	$B^1\Sigma^+$ ($v = 0$)	$B^1\Sigma^+$ ($v = 1$)	$C^1\Sigma^+$ ($v = 0$)
T_v	86916.4256 (12)	88972.9215 (22)	91918.9337 (14) 91918.83 (8)[c]
B_v	1.898 934 5 (75) 1.898 882 3 (41)[d]	1.873 949 (21) 1.874 146 (22)[e]	1.894 573 1 (76) 1.894 890 (11)[f] 1.895 0 (3)[c]
$D_v \times 10^6$	6.472 1 (88) 6.428 3 (26)[d]	7.395 (42) 6.937 (52)[e]	5.877 4 (77) 6.187 (12)[f] 6.0[c]

[a] All values in cm^{-1}. Uncertainties in parentheses represent one standard deviation in units of the last quoted digit. [b] T_v denotes the energy level separations between a given excited state and the $X^1\Sigma^+$ ($v = 0$, $J = 0$) ground state in $^{12}C^{17}O$. [c] After Ubachs *et al.*[22] [d] After Hakalla *et al.*[26] [e] After Hakalla *et al.*[27] [f] After Hakalla.[28]

contrast, for $A^1\Pi$ ($v = 1$) we observe distinct upward shifts of only the lowest rovibronic levels, with no significant effects on the Λ-doublings, despite the fact that the interaction is of a spin–orbit type. The reason is that this perturbation is caused by the lower lying $d^3\Delta_i$ ($v = 5$) state, which rapidly diverges with increasing rotation from the $^1\Pi$ partner. We deal with a similar situation for $A^1\Pi$ ($v = 4$), where the perturbation is caused by the $D^1\Delta$ ($v = 5$) level, but this is far less noticeable in the presented scale of the plot. It is worth considering the effect of Λ-doubling caused by a state of Σ symmetry. However, interactions with the $D^1\Delta$ and $d^3\Delta$ states induce perturbations of both e and f – parity levels, so do not result in Λ-doubling.

We should also notice the cases of spin–orbit interactions between $A^1\Pi$ and its $e^3\Sigma^-$, $a'^3\Sigma^+$, $d^3\Delta_i$ triplet perturbers, for which negligible Λ-doubling effects are observed, in spite of the

Table 13 Deperturbed equilibrium molecular constants of the $A^1\Pi$ state in $^{12}C^{17}O$[a,b,c]

Constant/state	$A^1\Pi$
Y_{00}	**−0.57**
Y_{10}	**1497.61**
	1497.94[d]
	1497.70[e]
	1501.18[f]
Y_{20}	**17.15**
	17.23[d]
	17.43[e]
	19.54[f]
$Y_{30} \times 10^2$	**6.69**
$Y_{40} \times 10^3$	[−8.82][d]
$Y_{50} \times 10^4$	[4.37][d]
Y_{01}	**1.574 11**
	1.574 41[d]
	1.574 59[e]
	1.574 33[f]
$Y_{11} \times 10^2$	**2.059**
	2.172[d]
	2.175[e]
	2.067[f]
$Y_{21} \times 10^3$	**−0.961**
	−0.953[f]
	−0.11[d]
	−0.10[e]
$Y_{31} \times 10^4$	[2.862][f]
$Y_{41} \times 10^5$	[−5.085][f]
$Y_{51} \times 10^6$	[5.1251][f]
$Y_{61} \times 10^7$	[−2.930][f]
$Y_{71} \times 10^9$	[8.846][f]
$Y_{81} \times 10^{10}$	[−1.106][f]
$Y_{02} \times 10^6$	**7.03**
	6.97[d]
	6.91[e]
$Y_{12} \times 10^7$	**1.13**
	1.22[e]
r_e	**1.233 87 (19)**
	1.233 781 (25)[g]
	1.233 753 (86)[h]

[a] All values in cm^{-1} except r_e [Å]. Uncertainties of the Dunham parameters have not been included, because these are not the fitted parameters and they do not reflect inter-parameter correlations. [b] Values given in square brackets were held fixed during the calculation. [c] Values calculated within this work are given in bold. [d] Isotopically recalculated from the $^{12}C^{18}O$ parameters given by Beaty *et al.*[52] [e] Isotopically recalculated from the $^{12}C^{16}O$ parameters given by Le Floch.[42] [f] Isotopically recalculated from the $^{12}C^{16}O$ parameters given by Field.[30] [g] Calculated by Field[30] for the $^{12}C^{16}O$ molecule. [h] Calculated by Beaty *et al.*[52] for the $^{12}C^{18}O$ isotopologue.

fact that the crossings occur within the observed $0 < J < 35$ region. We deal with such a case for the $A^1\Pi$, $v = 3$ and 5 levels where the perturbers are $d^3\Delta_i$ ($v = 8$), and $e^3\Sigma^-$ ($v = 8$), respectively. The reduced effects are in this case caused by the very small values of the vibrational integrals for the interacting levels in $^{12}C^{17}O$ (see Table 9). In turn, the *L*-uncoupling interactions between the $A^1\Pi$ state and $I^1\Sigma^-$, $D^1\Delta$ singlet states are usually much weaker. We can notice these interactions distinctly in Fig. 6b–d, where there are interactions of $A^1\Pi$ ($v = 2$) with $I^1\Sigma^-$ ($v = 3$), and $A^1\Pi$ ($v = 3$) with $D^1\Delta$ ($v = 4$) as well as $A^1\Pi$ ($v = 4$) with $I^1\Sigma^-$ ($v = 6$). In all these cases the largest term shifts do not exceed 0.5 cm^{-1}, which can be classified as weak interactions.

In Table 12, with the high accuracy of the results obtained, we notice a slight inconsistency of rotational constants B_v and D_v of $B^1\Sigma^+$ ($v = 0$ and 1) and $C^1\Sigma^+$ ($v = 0$) in relation to those that were calculated in our previous works.[26–28] This could be caused by the fact that the linear least-squares method in the version given by Curl and Dane[78] and Watson[79] takes no account of the impact of the Q(*J*) branches in the singlet–singlet fits. Improvement in the assignment of some of the heavily overlapped and/or extremely weak lines located in the region of strong and multistate perturbations, which was described in Section 2.1, could also be a reason for this inconsistency. It is worth noticing here that the deperturbation analysis conducted in this work was based on a global, three times more extensive experimental data set than was used in other works concerning the less-abundant $^{12}C^{17}O$ isotopologue.[26–28]

The present work also allowed for verification and improvement in the observed perturbations of the $A^1\Pi$, $v = 1$, and 2 rovibrational levels in $^{12}C^{17}O$ presented in ref. 26. For the $A^1\Pi$, $v = 1$ level, the $A^1\Pi$ ($v = 1$)~$D^1\Delta$ ($v = 1$) avoiding crossing occurs at $J = 26$–27, both for the e- and f-symmetry levels (see Fig. 6a). However, in the case of the $A^1\Pi$, $v = 2$ level, it turns out that in the perturbation analysis we must take into account small, but not negligible, impacts of the $a'^3\Sigma^+$ ($v = 11$) and $D^1\Delta$ ($v = 2$) states on its band origin and the fact that the maximum of the $A^1\Pi$ ($v = 1$)~$e^3\Sigma^-$ ($v = 4$; F_3) interaction for the e-symmetry levels falls at $J = 31$–32, and not at $J = 30$–31 as had been thought (see Fig. 6b).

It can be seen in Table 10 that the energy levels, T_v, for $A^1\Pi$ ($v = 1$) and $A^1\Pi$ ($v = 4$) have larger uncertainties than the remaining rovibrational levels of this state. This could be due to uncertainties derived from interactions with the $d^3\Delta_i$ ($v = 5$) and $D^1\Delta$ ($v = 5$) states, respectively. It is important to note that the rotational progressions of these states do not cross the $A^1\Pi$ ($v = 1$) and $A^1\Pi$ ($v = 4$) states. The effects of such interactions result in global energy shifts of the $A^1\Pi$ ($v = 1$, and 4) states, just as in the case of vibrational perturbations.[86] Thus, these interactions translate directly into uncertainties in T_v.

There is a very good agreement between the present and Le Floch's,[31] Field's,[30] and Field's *et al.*[32,87] values of the isotopologue independent electronic perturbation parameters ***a*** and ***b*** for the $A^1\Pi$~($d^3\Delta_i$, $e^3\Sigma^-$, $a'^3\Sigma^+$, $I^1\Sigma^-$, and $D^1\Delta$) interactions, highlighted in Tables 9 and 11. The obtained electronic perturbation parameters can be used to predict perturbations in other $A^1\Pi$ levels of all CO isotopologues. These parameters may be helpful in interpreting laboratory and astrophysical spectra of higher levels of the $A^1\Pi$ state.

5. Conclusion

Two different experimental methods, high-accuracy dispersive optical spectroscopy in the visible region and Fourier-transform spectroscopy in the vacuum ultraviolet region, were used to obtain high-resolution spectra of the $B^1\Sigma^+ \rightarrow A^1\Pi$, $B^1\Sigma^+ \leftarrow X^1\Sigma^+$, and $C^1\Sigma^+ \leftarrow X^1\Sigma^+$ systems in the less-abundant $^{12}C^{17}O$ isotopologue; a total of 429 high-accuracy transition

Table 14 Franck–Condon Factors (FCF) of the $B^1\Sigma^+$–$A^1\Pi$, $C^1\Sigma^+$–$A^1\Pi$, and $A^1\Pi$–$X^1\Sigma^+$ band systems in the $^{12}C^{17}O$ isotopologue

	$B^1\Sigma^+$			$C^1\Sigma^+$		
$A^1\Pi$ (v'')	$v' = 0$	$v' = 1$	$v' = 2^a$	$v' = 0$	$v' = 1$	$v' = 2^a$
0^a	9.0101×10^{-2}	0.2537	0.3176	9.0795×10^{-2}	0.2373	0.2914
1	0.1849	0.1736	7.3587×10^{-3}	0.1901	0.1741	1.3703×10^{-2}
2	0.2135	2.7840×10^{-2}	7.1057×10^{-2}	0.2195	2.8173×10^{-2}	6.2281×10^{-2}
3	0.1840	5.5201×10^{-3}	0.1122	0.1866	6.6188×10^{-3}	0.1167
4	0.1323	5.6103×10^{-2}	4.6893×10^{-2}	0.1311	6.2383×10^{-2}	5.2013×10^{-2}
5	8.3982×10^{-2}	9.9048×10^{-2}	1.5129×10^{-3}	8.0901×10^{-2}	0.1075	1.7551×10^{-3}
6^a	4.8926×10^{-2}	0.1082	1.3889×10^{-2}	4.5654×10^{-2}	0.1145	1.5607×10^{-2}

	$A^1\Pi$						
$X^1\Sigma^+$ (v'')	$v' = 0^a$	$v' = 1$	$v' = 2$	$v' = 3$	$v' = 4$	$v' = 5$	$v' = 6^a$
0	0.1173	0.2231	0.2333	0.1794	0.1139	6.3343×10^{-2}	3.2546×10^{-2}
1	0.2667	0.1511	8.9305×10^{-3}	2.6220×10^{-2}	9.5805×10^{-2}	0.1267	0.1156
2	0.2903	1.9746×10^{-3}	9.5116×10^{-2}	0.1123	2.7289×10^{-2}	1.8249×10^{-3}	4.1426×10^{-2}
3	0.2023	8.1391×10^{-2}	0.1102	3.4831×10^{-5}	6.3114×10^{-2}	8.7219×10^{-2}	3.3372×10^{-2}
4	0.1018	0.1985	3.1476×10^{-3}	9.1924×10^{-2}	5.7717×10^{-2}	4.1846×10^{-4}	4.8918×10^{-2}
5	3.9013×10^{-2}	0.1899	6.2494×10^{-2}	7.6121×10^{-2}	9.1741×10^{-3}	8.0194×10^{-2}	3.3475×10^{-2}
6	1.2109×10^{-2}	0.1134	0.1696	1.3827×10^{-5}	9.5519×10^{-2}	1.6287×10^{-2}	2.6512×10^{-2}
7	3.0502×10^{-3}	4.8889×10^{-2}	0.1699	7.3344×10^{-2}	4.2941×10^{-2}	3.5060×10^{-2}	6.4551×10^{-2}
8	6.6337×10^{-4}	1.6894×10^{-2}	0.1051	0.1637	5.1326×10^{-3}	8.6169×10^{-2}	7.7229×10^{-7}
9	1.2243×10^{-4}	4.6161×10^{-3}	4.5818×10^{-2}	0.1508	9.4368×10^{-2}	1.4775×10^{-2}	6.3127×10^{-2}
10	2.2279×10^{-5}	1.0469×10^{-3}	1.6225×10^{-2}	8.9287×10^{-2}	0.1601	2.3354×10^{-2}	6.0487×10^{-2}

[a] The vibrational levels, which have not been experimentally observed so far in $^{12}C^{17}O$.

frequencies were measured. The combined current data and our recent results,[26–28] in total 982 lines in 12 bands (B–A, C–A, B–X, C–X) and 15 bands consisting of extra-lines, were used to perform deperturbation analysis of the $A^1\Pi$ state in $^{12}C^{17}O$, taking into account the complete impacts of the $d^3\Delta_i$, $e^3\Sigma^-$, $a'^3\Sigma^+$, $I^1\Sigma^-$, and $D^1\Delta$ states. As a result the accurate perturbation model describes our experimental findings to the quantum level energies of accuracy.

Acknowledgements

R. Hakalla expresses his gratitude to the LASERLAB-EUROPE for support of this research (grant no. 284464 within the EC's Seventh Framework Programme). R. W. Field thanks the US National Science Foundation (grant no. CHE-1361865) for support of this research. A. Heays was supported by grant no. 648.000.002 from the Netherlands Organisation for Scientific Research (NWO) *via* the Dutch Astrochemistry Network. J. Lyons and G. Stark acknowledge support from the NASA Origins program. S. Federman was supported by NASA grants NNG 06-GG70G and NNX10AD80G to the University of Toledo. We are grateful to the general and technical staff of SOLEIL synchrotron for providing beam time under projects no. 20090021, 20100018, 20110121, and 20120653. The Rzeszów group would like to express their gratitude for the support of the European Regional Development Fund and the Polish state budget within the framework of the Carpathian Regional Operational Programme (RPPK.01.03.00-18-001/10) for the period of 2007–2013 through the funding of the Centre for Innovation and Transfer of Natural Science and Engineering Knowledge of the University of Rzeszów.

Notes and references

1 N. Neininger, M. Guelin, H. Ungerechts, R. Lucas and R. Wielebinski, *Nature*, 1998, **395**, 871–873.
2 J. Bally, A. A. Stark, R. W. Wilson and W. D. Langer, *Astrophys. J., Lett.*, 1987, **312**, L45–L49.
3 J. R. Lyons and E. D. Young, *Nature*, 2005, **435**, 317–320.
4 R. T. Garrod, S. L. Widicus Weaver and E. Herbst, *Astrophys. J.*, 2008, **682**, 283–302.
5 H. A. Weaver, P. D. Feldman, M. F. A'Hearn, N. Dello Russo and S. A. Stern, *Astrophys. J.*, 2011, **734**, L5–L9.
6 Q. M. Konopacky, T. S. Barman, B. A. Macintosh and C. Marois, *Science*, 2013, **339**, 1398–1401.
7 P. D. Feldman, E. B. Burgh, S. T. Durrance and A. F. Davidsen, *Astrophys. J.*, 2000, **538**, 395–400.
8 V. A. Krasnopolsky and P. D. Feldman, *Icarus*, 2002, **160**, 86–94.
9 P. D. Feldman, H. A. Weaver and E. B. Burgh, *Astrophys. J.*, 2002, **576**, L91–L94.
10 J.-C. Gérard, B. Hubert, J. Gustin, V. I. Shematovich, D. Bisikalo, G. R. Gladstone and L. W. Esposito, *Icarus*, 2011, **211**, 70–80.
11 E. F. Ladd, *Astrophys. J.*, 2004, **610**, 320–328.

12 J. G. A. Wouterloot, J. Brand and C. Henkel, *Astron. Astrophys.*, 2005, **430**, 549–560.
13 Y. Sheffer, D. L. Lambert and S. R. Federman, *Astrophys. J.*, 2002, **574**, L171–L174.
14 F. Bensch, I. Pak, J. G. A. Wouterloot, G. Klapper and G. Winnewisser, *Astrophys. J., Lett.*, 2001, **562**, L185–L188.
15 R. L. Smith, K. M. Pontoppidan, E. D. Young, M. R. Morris and E. F. Van Dishoeck, *Astrophys. J.*, 2009, **701**, 163–175.
16 R. Visser, E. F. van Dishoeck and J. H. Black, *Astron. Astrophys.*, 2009, **503**, 323–343.
17 S. R. Federman, D. L. Lambert, Y. Sheffer, J. A. Cardelli, B.-G. Andersson, E. F. Van Dishoeck and J. Zsargó, *Astrophys. J.*, 2003, **591**, 986–999.
18 P. Sonnentrucker, D. E. Welty, J. A. Thorburn and D. G. York, *Astrophys. J., Suppl. Ser.*, 2007, **168**, 58–99.
19 P. J. Encrenaz, P. G. Wannier, K. B. Jefferts, A. A. Penzias and R. W. Wilson, *Astrophys. J.*, 1973, **186**, L77–L80.
20 G. Guelachvili, *J. Mol. Spectrosc.*, 1979, **75**, 251–269.
21 P. Cacciani, W. Hogervorst and W. Ubachs, *J. Chem. Phys.*, 1995, **102**, 8308–8320.
22 W. Ubachs, P. C. Hinnen, P. Hansen, S. Stolte, W. Hogervorst and P. Cacciani, *J. Mol. Spectrosc.*, 1995, **174**, 388–396.
23 W. Ubachs, I. Velchev and P. Cacciani, *J. Chem. Phys.*, 2000, **113**, 547–560.
24 A. Du Plessis, E. G. Rohwer and C. M. Steenkamp, *J. Mol. Spectrosc.*, 2007, **243**, 124–133.
25 G. Stark, A. N. Heays, J. R. Lyons, P. L. Smith, M. Eidelsberg, S. R. Federman, J. L. Lemaire, L. Gavilan, N. de Oliveira, D. Joyeux and L. Nahon, *Astrophys. J.*, 2014, **788**, 67–80.
26 R. Hakalla, W. Szajna and M. Zachwieja, *J. Phys. B: At., Mol. Opt. Phys.*, 2012, **45**, 215102.
27 R. Hakalla, M. Zachwieja and W. Szajna, *J. Quant. Spectrosc. Radiat. Transfer*, 2014, **140**, 7–17.
28 R. Hakalla, *J. Quant. Spectrosc. Radiat. Transfer*, 2015, **164**, 231–247.
29 P. Cacciani, F. Brandi, I. Velchev, C. Lyngå, C.-G. Wahlström and W. Ubachs, *Eur. Phys. J. D*, 2001, **15**, 47–56.
30 R. W. Field, Ph.D. thesis, Harvard University, 1971.
31 A. C. Le Floch, F. Launay, J. Rostas, R. W. Field, C. M. Brown and K. Yoshino, *J. Mol. Spectrosc.*, 1987, **121**, 337–379.
32 R. W. Field, B. G. Wicke, J. D. Simmons and S. G. Tilford, *J. Mol. Spectrosc.*, 1972, **44**, 383–399.
33 C. Haridass, S. P. Reddy and A. C. Le Floch, *J. Mol. Spectrosc.*, 1994, **167**, 334–352.
34 B. A. Garetz, C. Kittrell and A. C. Le Floch, *J. Chem. Phys.*, 1991, **94**, 843–853.
35 R. Hakalla, W. Szajna, M. Zachwieja and R. Kepa, *Acta Phys. Pol., A*, 2012, **122**, 674–682.
36 R. Hakalla, M. Zachwieja and W. Szajna, *J. Phys. Chem. A*, 2013, **117**, 12299–12312.
37 R. Hakalla, *RSC Adv.*, 2014, **4**, 44394–44407.
38 M. Ostrowska-Kopeć, I. Piotrowska, R. Kępa, P. Kowalczyk, M. Zachwieja and R. Hakalla, *J. Mol. Spectrosc.*, 2015, **314**, 63–72.
39 P. H. Krupenie, *The Band Spectrum of Carbon Monoxide*, National Bureau of Standards, Washington, DC, 1966.
40 J. D. Simmons, A. M. Bass and S. G. Tilford, *Astrophys. J.*, 1969, **155**, 345–358.
41 R. W. Field, S. G. Tilford, R. A. Howard and J. D. Simmons, *J. Mol. Spectrosc.*, 1972, **44**, 347–382.
42 A. C. Le Floch, Ph.D. thesis, University Paris-Sud, 1989.
43 A. Le Floch, *J. Mol. Spectrosc.*, 1992, **155**, 177–183.
44 M. L. Niu, E. J. Salumbides, D. Zhao, N. de Oliveira, D. Joyeux, L. Nahon, R. W. Field and W. Ubachs, *Mol. Phys.*, 2013, **111**, 2163–2174.
45 E. J. Salumbides, M. L. Niu, J. Bagdonaite, N. de Oliveira, D. Joyeux, L. Nahon and W. Ubachs, *Phys. Rev. A*, 2012, **86**, 022510.
46 M. L. Niu, F. Ramirez, E. J. Salumbides and W. Ubachs, *J. Chem. Phys.*, 2015, **142**, 044302.
47 W. Ubachs, K. S. E. Eikema, W. Hogervorst and P. C. Cacciani, *J. Opt. Soc. Am. B*, 1997, **14**, 2469–2476.
48 N. de Oliveira, M. Roudjane, D. Joyeux, D. Phalippou, J.-C. Rodier and L. Nahon, *Nat. Photonics*, 2011, **5**, 149–153.
49 N. de Oliveira, D. Joyeux, D. Phalippou, J. C. Rodier, F. Polack, M. Vervloet and L. Nahon, *Rev. Sci. Instrum.*, 2009, **80**, 043101.
50 L. Nahon, N. De Oliveira, G. A. Garcia, J.-F. Gil, B. Pilette, O. Marcouillé, B. Lagarde and F. Polack, *J. Synchrotron Radiat.*, 2012, **19**, 508–520.
51 M. L. Niu, E. J. Salumbides, A. N. Heays, N. de Oliveira, R. W. Field and W. Ubachs, *Mol. Phys.*, 2016, **114**, 627–636.
52 L. M. Beaty, V. D. Braun, K. P. Huber and A. C. Le Floch, *Astrophys. J., Suppl. Ser.*, 1997, **109**, 269–277.
53 C. Haridass, S. P. Reddy and A. C. Le Floch, *J. Mol. Spectrosc.*, 1994, **168**, 429–441.
54 R. Kępa and M. Rytel, *J. Phys. B: At., Mol. Opt. Phys.*, 1993, **26**, 3355–3362.
55 R. Kępa, *J. Mol. Spectrosc.*, 1989, **135**, 119–130.
56 R. Kępa, *Can. J. Phys.*, 1988, **66**, 1012–1024.
57 R. Kępa, U. Domin and K. Porada, *Acta Phys. Pol., A*, 2003, **103**, 441–451.
58 R. Kępa, M. Ostrowska-Kopeć and I. Piotrowska, *J. Mol. Spectrosc.*, 2011, **266**, 104–112.
59 C. E. Moore and NIST ASD Team, *NIST At. Spectra Database*, National Institute of Standards and Technology, Gaithersburg, MD, 2014, http://physics.nist.gov/asd.
60 G. Tachiev and C. F. Fischer, *J. Phys. B: At., Mol. Opt. Phys.*, 2000, **33**, 2419–2435.
61 J. Baker and NIST ASD Team, *NIST At. Spectra Database*, National Institute of Standards and Technology, Gaithersburg, MD, 2014, http://physics.nist.gov/asd.
62 P. Zhao, W. Lichten, H. Layer, J. C. Bergquist and NIST ASD Team, *NIST At. Spectra Database*, National Institute of Standards and Technology, Gaithersburg, MD, 2014, http://physics.nist.gov/asd.
63 S. A. Mitchell and NIST ASD Team, *NIST At. Spectra Database*, National Institute of Standards and Technology, Gaithersburg, MD, 2014, http://physics.nist.gov/asd.
64 R. Kępa, M. Ostrowska-Kopeć, I. Piotrowska, M. Zachwieja, R. Hakalla, W. Szajna and P. Kolek, *J. Phys. B: At., Mol. Opt. Phys.*, 2014, **47**, 045101.
65 R. Bacis, *J. Phys. E: Sci. Instrum.*, 1976, **9**, 1081–1086.

66 R. Hakalla and M. Zachwieja, *J. Mol. Spectrosc.*, 2012, **272**, 11–18.
67 C. M. Western, *PGOPHER, a Program for Simulating Rotational, Vibrational and Electronic Structure*, University of Bristol, 2015, http://pgopher.chm.bris.ac.uk.
68 D. C. Morton and L. Noreau, *Astrophys. J., Suppl. Ser.*, 1994, **95**, 301–344.
69 B. A. Palmer and R. Engleman, *Atlas of the Thorium Spectrum*, Los Alamos Report LA-9615, Los Alamos Scientific Laboratory, Los Alamos, New Mexico, 1983.
70 W.-Ü. L. Tchang-Brillet, P. S. Julienne, J.-M. Robbe, C. Letzelter and F. Rostas, *J. Chem. Phys.*, 1992, **96**, 6735–6745.
71 A. N. Heays, G. D. Dickenson, E. J. Salumbides, N. De Oliveira, D. Joyeux, L. Nahon, B. R. Lewis and W. Ubachs, *J. Chem. Phys.*, 2011, **135**, 244301.
72 M. Eidelsberg, J. L. Lemaire, S. R. Federman, G. Stark, A. N. Heays, Y. Sheffer, L. Gavilan, J.-H. Fillion, F. Rostas, J. R. Lyons, P. L. Smith, N. de Oliveira, D. Joyeux, M. Roudjane and L. Nahon, *Astron. Astrophys.*, 2012, **543**, A69.
73 L. Gavilan, J. L. Lemaire, M. Eidelsberg, S. R. Federman, G. Stark, A. N. Heays, J.-H. Fillion, J. R. Lyons and N. de Oliveira, *J. Phys. Chem. A*, 2013, **117**, 9644–9652.
74 D. Bailly, E. J. Salumbides, M. Vervloet and W. Ubachs, *Mol. Phys.*, 2010, **108**, 827–846.
75 K. Yoshino and D. E. Freeman, *J. Opt. Soc. Am. B*, 1985, **2**, 1268–1274.
76 F. Brandi, I. Velchev, W. Hogervorst and W. Ubachs, *Phys. Rev. A*, 2001, **64**, 032505.
77 NIST ASD Team, *NIST At. Spectra Database*, National Institute of Standards and Technology, Gaithersburg, MD, 2014, http://physics.nist.gov/asd.
78 R. F. Curl and C. B. Dane, *J. Mol. Spectrosc.*, 1988, **128**, 406–412.
79 J. K. G. Watson, *J. Mol. Spectrosc.*, 1989, **138**, 302–308.
80 J. A. Coxon and P. G. Hajigeorgiou, *J. Chem. Phys.*, 2004, **121**, 2992–3008.
81 C. Kittrell and B. A. Garetz, *Spectrochim. Acta*, 1989, **45**, 31–40.
82 S. G. Tilford and J. D. Simmons, *J. Phys. Chem. Ref. Data*, 1972, **1**, 147–188.
83 K. P. Huber and G. Herzberg, *Constants of diatomic molecules*, Van Nostrand Reinhold, New York, 1979.
84 T. Bergeman and D. Cossart, *J. Mol. Spectrosc.*, 1981, **87**, 119–195.
85 J. L. Dunham, *Phys. Rev.*, 1932, **41**, 721–731.
86 G. Herzberg, *Molecular Spectra and Molecular Structure. I. Spectra of Diatomic Molecules*, reprinted 1989 by Krieger, Van Nostrand-Reinhold, Princeton, New Jersey, Malabar, 1950.
87 H. Lefebvre-Brion and R. W. Field, *The Spectra and Dynamics of Diatomic Molecules*, Elsevier Academic Press, Amsterdam, The Netherlands, 2004.
88 H. Lefebvre-Brion, *Can. J. Phys.*, 1969, **47**, 541–545.
89 R. J. Le Roy, *LEVEL 8.2: A Computer Program for Solving the Radial Schrödinger Equation for Bound and Quasibound Levels*, University of Waterloo Chemical Physics Research Report CP-663, 2014, http://leroy.uwaterloo.ca/programs/.
90 C. Jung, *FRACON-Programmdokumentation Quantenchemie*, Akademie der Wissenschaften der DDR, Berlin, 1979.
91 C. Jung and Z. Jakubek, *FRACONB-Programmdokumentation Quantenchemie FRACON (ver. B)*, Akademie der Wissenschaften der DDR and Pedagogical University of Rzeszów, Berlin – Rzeszów, 1988.
92 A. Le Floch, *Mol. Phys.*, 1991, **72**, 133–144.
93 G. Herzberg, J. D. Simmons, A. M. Bass and S. G. Tilford, *Can. J. Phys.*, 1966, **44**, 3039–3045.
94 K. F. Freed, *J. Chem. Phys.*, 1966, **45**, 4214–4241.
95 B. G. Wicke, R. W. Field and W. Klemperer, *J. Chem. Phys.*, 1972, **56**, 5758–5770.